Research Article

Mario A. Sandoval-Hernandez, Hugo Jimenez-Islas*, Hector Vazquez-Leal, Miriam L. Quemada-Villagómez, and María de la Luz Lopez-Gonzalez

Exploring homotopy with hyperspherical tracking to find complex roots with application to electrical circuits

https://doi.org/10.1515/math-2024-0115
received April 3, 2024; accepted December 3, 2024

Abstract: In the field of applied sciences, systems are frequently modeled using mathematical frameworks that include systems of nonlinear algebraic equations. Identifying their roots, whether real or complex, is of critical importance. The widespread use of complex numbers in science and engineering highlights the importance of accurately determining the complex roots of equations. This article presents a study in which the complex roots of a system of equations are identified through an approach that utilizes homotopy continuation, with the curve being traced using a hyperspherical path tracking technique. Furthermore, this article details five case studies on electrical networks where this method is applied to solve systems of equations containing imaginary coefficients to find mesh currents. The path tracking shows the behavior of system equation in each case study. Finally, an analysis of the precision of the solutions obtained in these case studies is provided, demonstrating an accuracy of up to 15 SDs in a single iteration during the refinement stage.

Keywords: homotopy continuation method, spherical path tracking methods, complex roots, multiple operating points, electrical circuits

MSC 2020: 0101, 65D25, 65H04, 65H10, 68W30

1 Introduction

In the history of complex numbers, a significant contribution was made by the mathematician Niccolò Tartaglia, who shared his secret solution techniques for solving equations with Girolamo Cardano, under the condition that Cardano would not disclose these techniques [1]. However, in 1545, Cardano published “Ars Magna”, a work in which he exposed methods for solving cubic equations [2,3]. This publication incited Tartaglia’s fury, as he accused Cardano of betrayal and dishonesty for failing to fulfill his promise.

*** Corresponding author: Hugo Jimenez-Islas,** Tecnológico Nacional de México en Celaya, Antonio García Cubas 600, Fovissste, 38010 Celaya, Gto, Mexico, e-mail: hugo.jimenez@itcelaya.edu.mx
Mario A. Sandoval-Hernandez: Centro de Bachillerato Tecnológico Industrial y de Servicios, No. 190. Av. 15 S/N esq. calle 11, col. Venustiano, Carranza, 94297 Boca del Río, Veracruz, Mexico; Tecnológico Nacional de México en Celaya, Antonio García Cubas 600, Fovissste, 38010 Celaya, Gto, Mexico; Universidad de Xalapa, Carretera Xalapa-Veracruz Km 2, No. 341, 91190 Xalapa, Veracruz, Mexico, e-mail: xallitic476@gmail.com
Hector Vazquez-Leal: Facultad de Instrumentación Electrónica, Universidad Veracruzana, Cto. Aguirre Beltrán S/N, Zona Universitaria, 91090 Xalapa, Veracruz, Mexico, e-mail: hvazquez@uv.mx
Miriam L. Quemada-Villagómez: Tecnológico Nacional de México en Celaya, Antonio García Cubas 600, Fovissste, 38010 Celaya, Gto, Mexico, e-mail: Miriam.quemada@itcelaya.edu.mx
María de la Luz Lopez-Gonzalez: Departamento de Enfermería y Obstetricia, Universidad de Guanajuato, Lascuráin de Retana, No. 5, Col. Centro, 36000. Guanajuato, Gto, Mexico, e-mail: mdll.lopezgonzalez@ugto.mx

Nonetheless, Lodovico Ferrari, a young mathematician and Cardano's assistant at the time, claimed that he was present during the meeting between the two mathematicians and asserted that no oath was taken [1].

Rafael Bombelli was familiar with the works of Girolamo Cardano on cubic equations, having studied his "Ars Magna". However, he found some concepts therein to be confusing and believed it was possible to elucidate them, making the information more accessible to the general public. Bombelli embarked on the development of a formal algebra to handle expressions of the form $a + b\sqrt{-1}$ [1,4]. In addition, in his 1572 work, Bombelli introduced calculus with negative numbers and established the rules for their addition and multiplication. His most significant contribution to algebra was the unconditional acceptance of the symbol $\sqrt{-1}$ as a legitimate number, marking a pivotal advance in the understanding and acceptance of complex numbers within the field of mathematics [1,4].

After the advancements made by Cardano and Bombelli, other mathematicians independently made significant contributions to the development of complex numbers. René Descartes, for instance, introduced the term "imaginary" in his work "La Géométrie" [5], marking the beginning of specific terminology to describe these numbers. On the other hand, John Wallis provided the first geometric interpretation of complex numbers, using line segments in the plane, which represented an important step toward their visual understanding [1].

Caspar Wessel, in his work "On the Analytical Representation of Direction: An Attempt Applied Chiefly to Solving Plane and Spherical Polygons" [6], demonstrated the geometric representation of an imaginary root of the form $a + bi$ using directed segments (vectors), including the addition and multiplication of these directed segments. This contribution was crucial for the geometric representation of complex numbers and their operations. Furthermore, Jean-Robert Argand proposed interpreting the value i as a rotation of 90 degrees in the coordinate plane, known as the Argand plane. In his essay, he also introduced, for the first time, the concept of modulus to indicate the magnitude of vectors and complex numbers, as well as the conventional notation for vectors with a horizontal arrow above the letters that indicate its endpoints [7].

Leonhard Euler standardized the notation for i to represent $\sqrt{-1}$ and used imaginary numbers to solve equations as well as in trigonometry applications [8,9]. In his work, Euler assigned the term "imaginary" to complex numbers, arguing that they were impossible quantities that only existed in the mind, due to their nontangible nature in the context of real numbers. On the other hand, Abraham de Moivre formulated the theorem bearing his name, which establishes the relationship between complex numbers and trigonometry, thus demonstrating their applicability and relevance in broader mathematical areas [10]. William Rowan Hamilton, in 1833, proposed a conceptualization of complex numbers as ordered pairs (a, b), where a and b are real numbers [11,12]. However, in electrical engineering, the notation for complex numbers underwent a significant change, wherein the imaginary unit is denoted by j. This convention was introduced and standardized by Charles Proteus Steinmetz in his seminal work "Complex Quantities and Their Use in Electrical Engineering" in 1893. Steinmetz's contribution greatly facilitated the analysis of alternating current (AC) circuits by simplifying complex calculations into straightforward algebraic operations. Consequently, he established the standardized use of phasor representation for complex numbers in educational texts on electrical engineering, employing the lower-case letter j to signify the 90-degree rotation operator in AC system analysis [13].

In this context, considering the historical background, complex numbers are characterized by their arithmetic properties and various forms of representation, among them, the phasor [14,15]. These numbers are situated in the complex plane, where the abscissa axis represents the real part and the ordinate axis signifies the imaginary part [14,15]. Their application spans a wide range, covering several fields from mathematics to various engineering disciplines. A notable example of their use is found in fractals, which are geometric objects characterized by a basic structure that, whether fragmented or irregular, repeats at multiple scales. This concept was introduced by mathematician Benoît Mandelbrot in 1977, using the term "fractal" from the Latin "fractus", meaning broken or fractured [16]. Among the most prominent fractal sets are the Mandelbrot and Julia sets, as highlighted by Monroy [14,17].

In the field of electricity and its subfields the applications of complex numbers have many applications, including the design of transmission lines in communications, where the Smith Chart is utilized for analyzing load impedances [18]. In signal processing, Fourier analysis employs the Fourier transform, which involves the

imaginary expression in the exponential function's argument, while the Fourier series in their complex form incorporates complex numbers [19]. In the qualitative theory of differential equations, the occurrence of complex roots in the eigenvalues of coefficient matrices plays a critical role in identifying behaviors such as centers and spirals, which can be stable or unstable [20]. In addition, in numerical analysis, complex numbers are utilized as starting points (SPs) in attraction basins to analyze the stability of numerical algorithms. They provide valuable information regarding the numerical instability of optimization methods, such as Newton-Raphson (N-R), the secant method, and Halley's method, among others [21–23]. Various authors have developed numerous analytical techniques using attraction basins. For instance, in [24], algorithms were developed for plotting the basins of attraction of fixed-points for a pair of bivariate rational functions using toroidal attraction basins. Moreover, in optics, complex numbers are employed to apply Fresnel integrals in diffraction phenomena [25]. In electrodynamics, they facilitate the study of the reflection and transmission of electromagnetic waves [26]. In the field of antenna design and behavior, complex numbers are applied in analyzing parameters such as impedance measurements, polarization, near-field and electromagnetic analysis, among others [27]. In electrical circuits, complex numbers are fundamental for calculating capacitive and inductive reactances, enabling the analysis of AC circuits [15]. Similarly, in power electrical systems, including industrial motors, networks, and three-phase circuits, they play a crucial role [28]. Furthermore, complex numbers are essential in the analysis of stability and frequency response [29], as well as in electronics for the analysis and synthesis of active filters [30,31]. In engineering, systems are modeled by equations and systems of differential, and occasionally algebraic, equations. Understanding the solutions to these equations is crucial, as they reveal the behavior of the system under given conditions. Specifically, for algebraic equations, the solutions can sometimes be complex. However, when dealing with equations that have real coefficients, these complex solutions appear in conjugate pairs [32].

There are several methods to determine complex roots in polynomial algebraic equations. For example, [32] details the Graeffe method as a technique for finding all the roots of an equation, whether real or imaginary. The Jenkins-Traub method is a globally convergent numerical algorithm that can find the real and complex roots of polynomials of a single variable [33]. Sandoval-Hernandez et al. [34] proposed a hybrid perturbation-N-R method to solve a nonlinear algebraic equation (NAEs) in circuit analysis, specifically to determine the bias points of a tunnel diode using real solutions. Dubeau and Gnang [35] employed the fixed-point and N-R methods to find solutions to nonlinear equations in the complex plane. In [36], Newton's method was adapted to polynomials with multiple roots in complex variables, applying it to Julia sets. On the other hand, Sandoval-Hernandez et al. [37] used a complex variable to obtain the general formula for solving quadratic equations. This formula is well known because it facilitates finding the different solutions of a quadratic equation, including solutions with complex numbers. In addition to the known methods for determining roots in equations, such as Regula Falsi or N-R, there are homotopy continuation algorithms that allow for solving systems of NAEs that can include transcendental functions. These are considered global convergence methods because they possess the ability to find solutions to nonlinear problems from almost any SP, theoretically ensuring that a solution will be reached regardless of the initial conditions. However, several authors have investigated the identification of complex roots through the application of homotopy continuation methods (HCMs). For instance, Gdawiec et al. [38] employed homotopy continuation for polynomial equations possessing both real and complex roots as a viable alternative to conventional iterative techniques. This approach was adopted to circumvent the issue of divergence.

In [39], an analysis was conducted on the SP utilizing the differential HCM to determine the conditions under which the convergence of these methods remains independent of the SP. This investigation aimed to facilitate the application of this technique to chemical engineering problems. However, the study also explored the behavior of the homotopic path in a case study where certain roots could not be identified due to the homotopic route encountering a region within the complex domain. Following this, in [40], the implementation of continuation homotopy was conducted to determine the roots of polynomial equations with real coefficients by substituting the complex variable $z = x + yi$ to derive a homotopy for the real part and another for the imaginary part, with applications in chemical engineering. Furthermore, in [38–40], the authors have focused solely on finding complex roots for a polynomial equation using continuation homotopy without conducting any error or significant digit (SD) analysis. On the other hand, [40] presented the plotting of

homotopic tracking for the real and imaginary parts separately against the homotopic parameter τ. Furthermore, Vazquez-Leal et al. [41] proposed the biparameter homotopy with an automated stop criterion, aiming to achieve the lowest number of iterations necessary to complete the tracing of a symmetrical branch. The multiparametric homotopy utilizes multiple parameters, providing greater flexibility in solving systems of nonlinear equations and reducing computation times. In [42], the use of predictor vectors (without correction vectors) was proposed to find the solution to several systems of NAEs with multiple solutions, employing lower central processing unit (CPU) time compared to standard homotopic tracking algorithms.

Due to its ability to find multiple roots in NAEs, homotopy has broad applications in chemical engineering. For example, chemical process control problems and chemical reactions often involve nonlinear equations with multiple solutions, heat diffusion processes, exothermic reaction, natural convection of air in a 2D square cavity at a steady state, and homotopic methods enable the identification of all possible solutions, allowing the selection of the most appropriate one [43–45], solution vectors for an elliptic system of 2D partial differential equations for natural convection [46]. Likewise, homotopy methods have been applied in electronic circuits to find the polarization point in nonlinear circuits [47–49], and in electronics to determine the operating point in circuits with transistors [50–56]. In addition, they have been used in the design of simulators for electronic circuits [57,58].

Recently, Vazquez-Leal and his research team [59] initiated a new line of research in robotics, emphasizing the importance of understanding the behavior of the homotopic path that models the movement trajectory of a mobile device. In [60], homotopy with hyperspherical tracking was applied for route planning, solving an NAE system that models the obstacles to be avoided. Furthermore, in [61,62], homotopy with hyperspherical tracking was utilized in a collision-free trajectory planning algorithm for robotic arms, addressing an NAE system that models the robot's workspace.

This paper introduces the implementation of continuation homotopy with hyperspherical tracking [44,63], implemented in Maple using symbolic programming. This approach enables comprehensive tracking, considering both the real and imaginary parts integrally without their separation, aimed at resolving various systems of equations with imaginary coefficients within the context of electrical engineering problems. This method facilitates the exploration and examination of the solutions obtained, as well as the analysis of the behavior of their homotopic paths. Furthermore, it enhances the body of literature [64,65] dedicated to the determination of real roots of systems of equations through the use of continuation homotopy.

This paper is organized as follows: Section 2 introduces a brief historical note about continuation homotopy. Section 3 introduces the continuation homotopy method with hyperspherical tracking. Section 4 presents five case studies; the first involves a system of polynomial equations, while the subsequent case studies focus on solving systems of equations applied to electrical circuits. Section 5 details the numerical simulations and discussions. Finally, Section 6 outlines the conclusions of this work.

2 A brief historical review of HCMs

The formal origins of homotopy trace back to the work of French mathematician Henri Poincaré (1854–1912), widely regarded as the founder of algebraic topology. In his series of publications entitled "Analysis Situs", Poincaré introduced the foundational concepts that would later develop into the theory of homotopy [66]. To fully contextualize the state of the art during Poincaré's era, it is essential to understand the problem that sparked his interest in topology.

To understand the foundation of homotopy, it is essential to review the transformations involved. Topology studies the properties of geometric bodies that remain invariant under continuous transformations and their inverses [67]. This concept focuses on specific points that do not change when geometric bodies are contracted, expanded, or deformed [68,69]. In Figure 1, the points on the cube are relocated without generating new points during compression or expansion, illustrating a continuous transformation. This property, where $f(x)$ does not introduce changes and maintains continuity, is referred to as a "homeomorphism" [70]. While it is easy to visualize deformation in simple shapes like a cube, the correspondence in more complex bodies

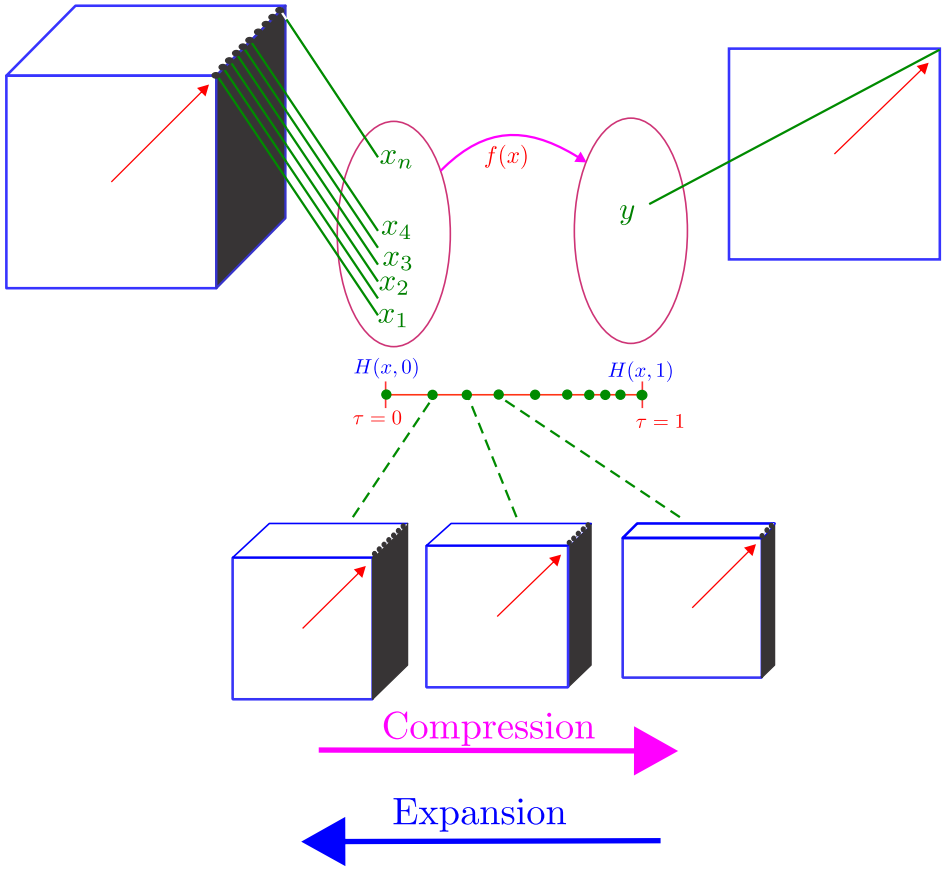

Figure 1: Schematic diagram of Homotopy between two geometric bodies.

is less apparent [71]. This introductory concept provides a basis for understanding homotopy methods as a tool for solving algebraic equations.

Poincaré's contributions to topology were of immense importance, as he introduced algebraic tools that enabled mathematicians to study abstract geometric properties without relying on classical geometric intuition. Homotopy became a cornerstone of this approach, offering an algebraic framework for addressing complex topological problems [70].

One of the first significant practical advances derived from homotopy theory was the fixed-point theorem, formulated by the Dutch mathematician Brouwer [72,73]. This theorem states that any continuous function mapping a closed sphere onto itself must have at least one fixed-point, meaning a point that remains invariant under the function. This theorem forms the philosophical link between Poincaré's homotopy theory and the development of tools for solving algebraic equations and systems of equations. García and Zangwill further elaborate on the concept introduced by Brouwer [74].

In the context of homotopy theory, Brouwer's theorem established a direct connection between the abstract concepts of algebraic topology and the solution of concrete problems in NAEs. This theorem marked homotopy's first major application in developing methods for solving systems of equations, a line of research that would be extensively explored in the following decades [74].

As homotopy theory evolved, new tools were developed to tackle more complex problems. In 1934, French mathematicians Jean Leray and Jules Schauder introduced the concept of "topological degree" in their work "Topologie et équations fonctionnelles" as an extension of homotopy theory for systems of nonlinear equations [75]. The topological degree is an algebraic invariant that measures the "number of solutions" of a nonlinear equation by analyzing the signs of the derivatives or Jacobians of the functions involved.

The topological degree was crucial in formalizing HCMs. These methods involve continuously transforming a system of nonlinear equations into a simpler version with a known solution and then following

this transformation until the solution of the original system is obtained. This is accomplished through a homotopic function, which links the solutions of the original system to those of the simplified system via the homotopic variable τ, ranging from $\tau = 0$ to $\tau = 1$. The topological degree ensures that the number of solutions remains constant throughout the transformation, enabling the tracing of all possible solutions of the system [67,68].

In the 1950s, homotopy methods progressed with the development of corrector-predictor methods, proposed by Ficken in 1951 in his article "The Continuation Method for Functional Equations" [76]. These methods combined solution prediction with iterative correction using the N-R method to ensure convergence. One major improvement was the introduction of tangent predictors to the homotopic curve. In 1961, Haselgrove advanced this approach by applying Newton's Method as a corrector in systems of nonlinear equations, detailed in his work "The Solution of Non-Linear Equations and of Differential Equations with Two-Point Boundary Conditions", he details the use of Newton's n-dimensional algorithm in the solution of systems of n-NAEs with $n + 1$ variables (n variables, plus the homotopic parameter τ) [77]. His contribution provided a general description of a predictor-corrector continuation algorithm, expanding on the earlier work of Davidenko [78], they are as follows:

- ♠ Horizontal Predictors: Proposed by Lahaye in 1934 [79] and later used by Davidenko in 1953 [78,80], these methods sequentially increase the homotopy parameter. However, they are less efficient when there are returns along the homotopy path, as they require precise control of step size to ensure accuracy.
- ♠ Differential Predictors: Introduced by Haselgrove in 1961 [77], they use the slope of the homotopic path to predict the next point to correct. Compared to horizontal predictors, they offer predictions closer to the actual path, facilitating convergence on local correction methods.
- ♠ Polynomial Predictors: Proposed by Rheinboldt in 1975 [81], these methods use polynomial functions, such as Lagrange and Hermite polynomials, to predict the next point on the curve. Although they offer greater accuracy compared to earlier methods, their effectiveness decreases on curves with returns.
- ♠ Lagrange Polynomials: Implemented by Rheinboldt in 1975 to enhance predictions in continuation processes [81]. Hermite Polynomials: Mentioned by Deufhard in 1979 as a potential option, though no practical applications were provided [82].
- ♠ Closed Surfaces: The use of closed surfaces as predictors has had limited practical application in homotopy methods and was first introduced by Lyness and McHugh in 1963 [83]. They employed "hypercubes" in numerical integration, comparing their method to traditional techniques like Simpson and Euler-Maclaurin, showing improved precision [84]. After 1963, few publications have reported on closed trajectories as a prediction method for homotopy curves.
- ♠ Hyperspherical Path Tracking: Jiménez-Islas reviewed the closed surface approach in 1985, conducting various analyses. He was the first to propose hyperspherical tracking ad hyperspherical tracking with variable radius in his 1988 master's thesis, "Paquete Computacional para la Solución de sistemas de ecuaciones no lineales" [85], at Instituto Tecnológico de Celaya, without knowledge of Ushida's work [86]. Islas published his results until 1996, applying them to chemical engineering [44].

  On the other hand, since 1976, Ushida and Chua worked on solving nonlinear equations in circuit theory using continuation homotopy to address sharp turning points in solution curves [48,49]. In their 1984 article "Tracing Solution Curves of Nonlinear Equations with Sharp Turning Points" [86], they introduced an additional equation for homotopy formulation using arc-length. Previously, this idea had been used in other works [47–49,87].

  The contribution in this article [86] was to solve the system of n nonlinear equations in $(n + 1)$ variables, directly incorporating the equation for arc-length using the implicit backward-differentiation formula [88,89]. Yamamura later extended the work of Ushida and Chua, unaware of Islas' contributions [85]. In 1990, Yamamura discussed this work with Inoue from Sanyo Electric Company, and in 1993, he published results using hyperspheres in homotopy with applications in electronic circuits [90].

From 1960s, homotopy methods advanced with the introduction of arc-length parameterization, proposed by Klopfenstein in 1961, which improved solution tracking and mitigated issues related to singularities in the Jacobian [91]. This technique provided greater control over curve tracking. In addition, homotopy methods

faced challenges with bifurcations, where solution curves split into multiple branches, signaling changes in solution stability [92]. Alexander and Yorke generalize the HCM in "The Homotopy Continuation Method: Numerically Implementable Topological Procedures" [93], freeing it from its dependence on degree and broadening its application to problems beyond traditional degree arguments, particularly in locating bifurcating sets in nonlinear equations.

Homotopy methods have continued to evolve with the introduction of other techniques to improve their robustness and applicability. For example, Chow et al. [94] presented an approach based on a transversality theorem called "the Parametrized Sard Theorem". This work gave solutions to problems in which the topological scheme is more complicated, for example, finding the Brouwer fixed-point, finding solutions of two point boundary problems for second-order ordinary differential equations in R^n, among others. In [95], the Chow-Yorke algorithm [96] was applied to problems such as the elliptic porous slider, the squeezing of a viscous fluid between parallel plates, the squeezing of a viscous fluid between elliptic plates, and viscous flow between rotating discs with injection on the porous disc, among others. These problems range from fairly simple to extremely difficult, and Newton-type methods either partially or totally failed on all of them. In [97], a method was introduced for solving systems of polynomial equations, specifically when these systems had to be solved repeatedly with different sets of values. This method, referred to as "cheater's homotopy", employed a path-tracking technique to find all possible solutions, significantly improving computational efficiency. Unlike traditional methods, which required substantial computational resources based on the overall complexity of the equations, this approach targeted the actual number of solutions, resulting in faster and more practical performance for a variety of applications.

Over time, various homotopy methods have been developed, including Newton homotopy [98], fixed-point homotopy [99,100], affine homotopy [84], Combined fixed-point Newton homotopy [101], probability one homotopy [102], and multiparameter homotopies [103]. In all cases, homotopies find a solution when the homotopic parameter $\tau = 1$. However, in previous years, obtaining the exact solution at $\tau = 1$ was challenging due to numerical errors in the algorithms, requiring the roots to be calculated experimentally. In his thesis, Islas proposed refining the solution using N-R when the neighborhoods of $\tau = 1$ were reached, before and after this value. His proposal is included in GW-BASIC code in the appendix of his work [85]. However, in 1996, Sosonkina introduced the zero-finding strategy in his work "Note on the End Game in Homotopy Zero Curve Tracking" [104] (without knowledge of Islas' work). Continuation methods were further improved by the introduction of this strategy, which is crucial for ensuring convergence along the homotopy path, as the process may fail to find solutions without it.

3 Basic concepts of HCMs

Solving systems of NAEs can be challenging using traditional approaches such as the N-R method. The N-R method requires an initial approximation of the solution to begin the process. However, it is well known that for some cases, the N-R method may not converge to a solution from any SP. Often, finding an appropriate initial guess is not straightforward or even feasible. As a result, the reliability of the N-R method for solving all types of problems cannot be assured. An alternative strategy to overcome this limitation involves employing HCM. The HCM methods represent a continuous deformation from a basic problem (easy to solve) to the target problem (difficult to solve), facilitating a smoother pathway to finding solutions.

HCMs are utilized to locate multiple solutions within systems of NAEs (n equations with n unknowns) of the form

$$f(\mathbf{x}) = 0, \quad \text{where } f : \mathbb{R}^n \to \mathbb{R}^n. \tag{1}$$

The HCMs introduce a perturbation in the system $f(x)$ by incorporating a function $G(x)$ and a homotopic parameter τ. In this manner, the original system is transformed into a homotopic system expressed as follows:

$$H_i(\mathbf{x}, \tau) = H_i(f(\mathbf{x}), \tau) = \tau f(\mathbf{x}) + (1 - \tau)G(\mathbf{x}) = 0, \tag{2}$$

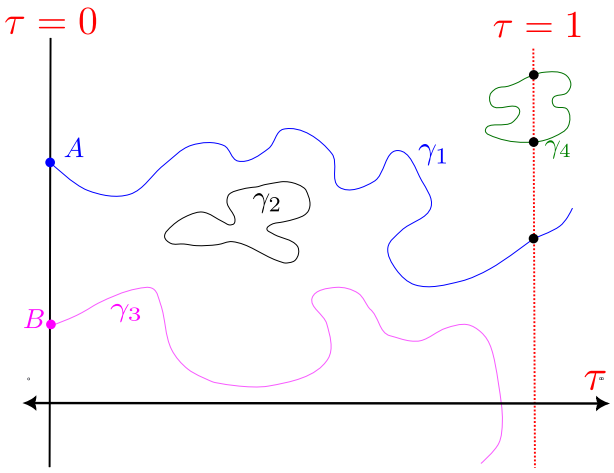

Figure 2: Family of homotopy curves.

where $H(\mathbf{x}, \tau) : \mathbb{R}^{n+1} \to \mathbb{R}^n$, $i = 1 \ldots, n$, and τ is the homotopy parameter. The function $G(\mathbf{x})$ exhibits a known solution or is easily solvable.

Equation (2) represents any homotopy formulation that meets the following conditions:

- If $\tau = 0$ and $H(\mathbf{x}, 0) = G(\mathbf{x}) = 0$, then a solution for H is known or can be easily found using numerical methods.
- If $\tau = 1$ and $H(\mathbf{x}, 1) = f(\mathbf{x}) = 0$, then the solution of the original system is obtained.

The deformation process of the system initiates at $\tau = 0$, and the solutions of interest emerge upon reaching $\tau = 1$ and beyond. Each intersection at $\tau = 1$ constitutes a solution vector for (2). The mapped solutions are presented as a family of curves, γ, as referenced in [39,44,105]. Figure 2 displays four examples of homotopic continuous curves. Here, γ_1 represents a successful case, transitioning from the SP A at $\tau = 0$ to the solution at $\tau = 1$, whereas the other paths illustrate instances where the HCM method does not succeed. It is noteworthy that the trajectory γ_4 is capable of identifying solutions; however, it remains isolated from the initial point, making it impossible to connect it with γ_1.

The selection of $G(\mathbf{x})$ dictates the formulation of the homotopy. In this study, we employ Newton's homotopy, defined as $G(\mathbf{x}) = f(\mathbf{x}) - f(\mathbf{x}_0)$, i.e., the function $f(\mathbf{x})$ minus the functions evaluated at $\mathbf{x}_0$ [44]. Thus, by substituting Newton's homotopy into (2), we obtain

$$H_i(\mathbf{x}, \tau) = f(\mathbf{x}) - (1 - \tau)G(\mathbf{x}), \quad \mathbf{x} \in \mathbb{R}^n, \tag{3}$$

where $\mathbf{x}_0$ is the SP.

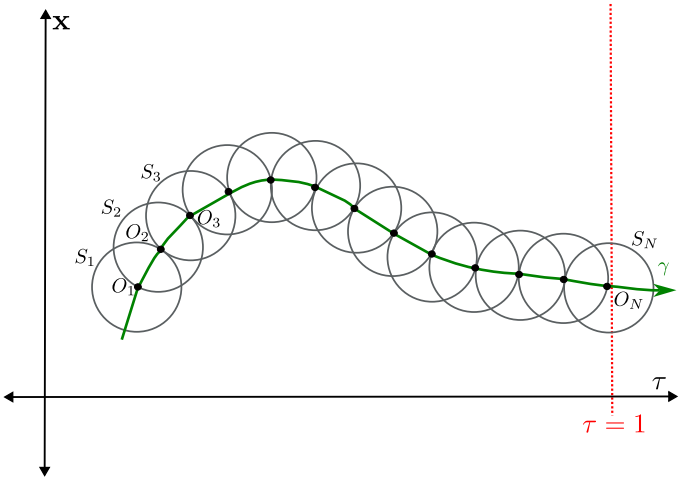

Figure 3: Potential homotopy path.

The application of HCM requires the implementation of a technique to map the homotopic path [44]. For example, when a hypersphere S_2 with radius r and center O_2 is located on the homotopy path, its contour is required to intersect the homotopy curve at two points, O_1 and O_3, as shown in Figure 3. The center O_1 is the center of the hypersphere of the previous iteration, O_3 is the center of the hypersphere of the next iteration as depicted in Figure 3.

3.1 Path tracking of the homotopy trajectory

The formulation of a homotopy system involves n equations and $n + 1$ variables, that is, n variables of the system plus the homotopy parameter τ [44,60]. Therefore, in the context of the hyperspherical path tracking technique, we must include an additional equation known as the hypersphere, which is given by

$$S_i(\mathbf{x}, \tau) = \sum_{k=1}^{n} (x_k - c_k)^2 + (\tau - c_{n+1})^2 - r^2 = 0, \tag{4}$$

where r is the radius and (c_k, c_{n+1}) is the center of the sphere in the homotopy path. $i = 1, \ldots, N$ are iterations for the hyperspheres $S_i(\mathbf{x}, \tau)$ used to trace the homotopic path. By using (3) and (4), we have a system with $n + 1$ equations given by

$$H_s(\mathbf{x}, \tau) = \begin{cases} H_1(\mathbf{x}, \tau) = 0, \\ H_2(\mathbf{x}, \tau) = 0, \\ \vdots \\ H_n(\mathbf{x}, \tau) = 0, \\ S_i(\mathbf{x}, \tau) = 0. \end{cases} \tag{5}$$

For the case of n variables, the homotopic path γ shown in Figure 3 is formed by the centers $O_1, O_2, O_3, \ldots, O_N$ and these are calculated with help of equation (4) of the hypersphere S_i. To find the coordinates of the centers $O_i(c_k, c_{n+1})$ of the S_i must be solve the system (5) (with variables $\mathbf{x}, \tau$) by iterating N times in the path following.

During the tracking algorithm, the center of (4) must be updated at each tracking step and resolved for (5). Subsequently, spherical tracking is conducted, as depicted in Figure 3. Initially, we center the first hypersphere at the SP of the homotopy. Next, a prediction step is performed to approach the next point, and a correction step ensures the path following of the homotopy curve. Finally, the center of the hypersphere is updated at (5), and the process is repeated until the procedure reaches $\tau = 1$, where interpolation and refinement steps are executed to find a solution for $f(\mathbf{x}) = 0$. Thereafter, the procedure continues until another root is found or the maximum number of iterations is reached. During this process, τ can cross $\tau = 1$ several times from left to right and *vice versa*.

The predictor-corrector scheme enables the spherical algorithm (SA) to accurately track the homotopy curve γ. Figure 4 illustrates the behavior of the predictor-corrector scheme. The Euler predictor establishes a tangent vector $(\mathbf{x}_p, \tau_p)$ at the point $(\mathbf{x}_i, \tau_i)$ along the homotopy path. Subsequently, the predictor point is determined at the intersection of the sphere S_i with the tangent vector. The N-R method is then employed as a corrector to ascertain the intersection point $(\mathbf{x}_{i+1}, \tau_{i+1})$ between the homotopy path and the sphere of radius r. This yields a point in proximity to the solution of the homotopy system for the subsequent tracking step. The Euler predictor point utilized in SA is expressed as follows:

$$(\mathbf{x}_p, \tau_p) = (\mathbf{c}_x, c_\tau) + r\|\vec{v}_p\|, \tag{6}$$

where $(\mathbf{x}_p, \tau_p)$ is the predictor point, $(\mathbf{c}_x, c_\tau)$ is the center of the sphere, r is the radius of the sphere, and $\vec{v}_p$ is the tangent vector.

The N-R method is used to correct the predictor point to a point on the homotopy path γ. The N-R corrector is described by

$$(\mathbf{x}_{j+1}, \tau_{j+1}) = (\mathbf{x}_j, \tau_j) - [J(\mathbf{x}_j, \tau_j)]^{-1} H_s(\mathbf{x}_j, \tau_j), \tag{7}$$

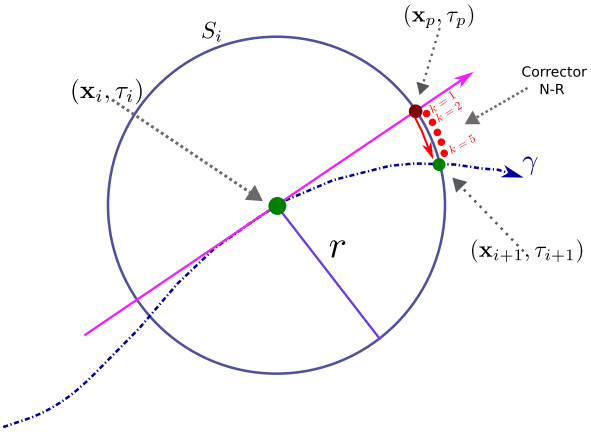

Figure 4: N-R corrector in spherical tracking.

where $j = 0, 1, 2, \ldots, n$ iteration, and $(\mathbf{x}_j, \tau_j)$ is the point updated in each iteration until reaching a final value; this final value can be regarded as the solution. $[J(\mathbf{x}_j, \tau_j)]^{-1}$ denotes the inverse Jacobian of H_s evaluated at the point $(\mathbf{x}_j, \tau_j)$ for each jth iteration. This iterative method necessitates an appropriate SP to obtain the solution in a minimum number of iterations. Therefore, for the first iteration, $j = 0$, $(\mathbf{x}_j, \tau_j) = (\mathbf{x}_p, \tau_p)$. The N-R method is reiterated until it reaches a maximum number of iterations $j_{\max}$ or it converges to a solution $(\mathbf{x}_{i+1}, \tau_{i+1})$ with a minimal margin of error, as depicted in Figure 4.

3.2 Implementation of homotopy with spherical path tracking

The predictive section of the hyperspherical path tracking methodology presented in [44] forms the core of the strategy. The predictive homotopic path tracking is applied to a system of nonlinear equations derived from a set of n deformed algebraic equations with Newton's homotopy. By parameterizing equation (3) with parameter p, the homotopic functions $H_i(\mathbf{x}, \tau)$ is defined as $H_i(\mathbf{x}(p), \tau(p))$, is defined as follows:

$$H_i(\mathbf{x}(p), \tau(p)) = f(\mathbf{x}(p)) - (1 - \tau(p))f(\mathbf{x}_0), \quad \mathbf{x} \in \mathbb{R}^n. \tag{8}$$

It is noteworthy that the addition of the parameter p allows visualization regardless of the number of equations that the nonlinear algebraic system, solved by $f(\mathbf{x})$, has. Therefore, the generation of the homotopic path is defined by $H^{-1}(p, \tau(p))$. The homotopic route tracking is done by generating a tangent vector, $\frac{\partial \tau}{\partial p}$, which passes through the initial point $\mathbf{x}_0$, and allows us to predict the point $\mathbf{x}_1$. The slopes ∂p are defined by calculating the partial derivatives of each homotopic function, $H_i(\mathbf{x}(p), \tau(p))$. We define the matrix $\mathbf{H}$ as follows:

$$\mathbf{H} = \begin{bmatrix} \frac{\partial H_1}{\partial x_1}\frac{\partial x_1}{\partial p} & \cdots & \frac{\partial H_1}{\partial x_n}\frac{\partial x_n}{\partial p} & \frac{\partial H_1}{\partial \tau}\frac{\partial \tau}{\partial p} \\ \frac{\partial H_2}{\partial x_1}\frac{\partial x_1}{\partial p} & \cdots & \frac{\partial H_2}{\partial x_n}\frac{\partial x_n}{\partial p} & \frac{\partial H_2}{\partial \tau}\frac{\partial \tau}{\partial p} \\ \vdots & \ddots & \vdots & \vdots \\ \frac{\partial H_n}{\partial x_1}\frac{\partial x_1}{\partial p} & \cdots & \frac{\partial H_n}{\partial x_n}\frac{\partial x_n}{\partial p} & \frac{\partial H_n}{\partial \tau}\frac{\partial \tau}{\partial p} \end{bmatrix}, \quad \mathbf{H} \in \mathbf{M}_{n,n+1}\mathbb{R}. \tag{9}$$

By expressing equation (9) as a system of equations in its matrix form, we have

$$\begin{bmatrix} \frac{\partial H_1}{\partial x_1} & \cdots & \frac{\partial H_1}{\partial x_n} \\ \vdots & \ddots & \vdots \\ \frac{\partial H_n}{\partial x_1} & \cdots & \frac{\partial H_n}{\partial x_n} \end{bmatrix} \begin{bmatrix} \frac{\partial x_1}{\partial p} \\ \vdots \\ \frac{\partial x_n}{\partial p} \end{bmatrix} = - \begin{bmatrix} \frac{\partial H_1}{\partial \tau}\frac{\partial \tau}{\partial p} \\ \vdots \\ \frac{\partial H_n}{\partial \tau}\frac{\partial \tau}{\partial p} \end{bmatrix}. \tag{10}$$

By applying Cramer's rule in equation (10), we have the solution to the system

$$\begin{aligned} \frac{\partial x_1}{\partial p} &= \frac{\begin{Vmatrix} -\frac{\partial H_1}{\partial \tau}\frac{\partial \tau}{\partial p} & \cdots & \frac{\partial H_1}{\partial x_n} \\ \vdots & \ddots & \vdots \\ -\frac{\partial H_n}{\partial \tau}\frac{\partial \tau}{\partial p} & \cdots & \frac{\partial H_n}{\partial x_n} \end{Vmatrix}}{||\mathbf{H}||}, \\ &\vdots \\ \frac{\partial x_n}{\partial p} &= \frac{\begin{Vmatrix} \frac{\partial H_1}{\partial x_1} & \cdots & -\frac{\partial H_1}{\partial \tau}\frac{\partial \tau}{\partial p} \\ \vdots & \ddots & \vdots \\ \frac{\partial H_n}{\partial x_1} & \cdots & -\frac{\partial H_n}{\partial \tau}\frac{\partial \tau}{\partial p} \end{Vmatrix}}{||\mathbf{H}||}, \end{aligned} \tag{11}$$

where $||\mathbf{H}||$ is the determinant of the system. Simplifying using properties of the determinants, each variable is expressed

$$\begin{aligned} \frac{\partial x_1}{\partial p} &= (-1)(-1)\frac{\partial \tau}{\partial p}\frac{||\mathbf{H_1}||}{||\mathbf{H}||}, \\ \frac{\partial x_2}{\partial p} &= (-1)\frac{\partial \tau}{\partial p}\frac{||\mathbf{H_2}||}{||\mathbf{H}||}, \\ &\vdots \\ \frac{\partial x_k}{\partial p} &= (-1)(-1)\frac{\partial \tau}{\partial p}\frac{||\mathbf{H_k}||}{||\mathbf{H}||}, \end{aligned} \tag{12}$$

where $||\mathbf{H_k}||$, $k = 1, 2, \ldots, n$ is the determinant from which column k has been removed, according to Cramer's rule. To determine $\frac{\partial \tau}{\partial p}$, we must substitute $\frac{\partial \tau}{\partial p} = (-1)||\mathbf{H}||$ into (12), and by generalizing for any number of variables, $\frac{\partial x_i}{\partial p}$, we obtain

$$\begin{aligned} \frac{\partial x_k}{\partial p} &= (-1)^k||\mathbf{H_k}||, \\ &\vdots \\ \frac{\partial \tau}{\partial p} &= (-1)^{n+1}||\mathbf{H_{n+1}}||. \end{aligned} \tag{13}$$

In this way, by rewriting (13) in the form of a column vector, a general expression for the slopes is obtained

$$\dot{\mathbf{y}}_\mathbf{k} = (-1)^k||\mathbf{H_k}|| \begin{bmatrix} \frac{\partial x_k}{\partial p} \\ \vdots \\ \frac{\partial \tau}{\partial p} \end{bmatrix}, \quad k = 1, \ldots, n+1. \tag{14}$$

Equation (14) expresses the slopes for each of the variables in the homotopic path γ, being essential for calculating each predictor vector. To determine the prediction vectors, we must consider the slopes of the homotopic path calculated with (14) and use Euler's predictor algorithm. In this case, it is expressed as

$$\begin{aligned} \mathbf{x}_p &= \mathbf{x}_0 + \Delta p \frac{\mathrm{d}\mathbf{x}}{\mathrm{d}p}, \\ \tau_p &= \tau_0 + \Delta p \frac{\mathrm{d}\tau}{\mathrm{d}p}, \end{aligned} \tag{15}$$

where $\mathbf{x_p}$ and τ_p are the prediction values obtained by the Euler predictor, which will be found on the surface of the hypersphere of radius r. To calculate the horizontal advance Δp, equations (15) are used, adding the equation of the hypersphere. In this way, we have

$$\Delta p = \pm \frac{r^2}{\sqrt{\sum_{k=1}^{n} \left[\frac{\partial x_k}{\partial p}\right]^2 + \left[\frac{\partial \tau}{\partial p}\right]^2}}. \tag{16}$$

The sign will depend on the direction of tracking to the right or left, that is, in a positive or negative direction. In this way, it is possible to calculate the prediction for $\mathbf{x_p}$ and τ according to (15). To calculate the corresponding point p to the horizontal advance of the homotopic path, the equation will be used

$$p = p_0 + \Delta p. \tag{17}$$

Once the prediction vectors have been calculated, they now serve as the new initial values to begin the hyperspherical correction procedure, whose objective is to find the intersection between the hypersphere and the homotopic path, as shown in Figure 4. This procedure is carried out using the N-R method to solve the homotopic equations of the system, described by (3), and with the equation of the hypersphere (4). The N-R method, in two or more dimensions, requires the Jacobian matrix and a vector with the function evaluated at an initial point $(\mathbf{x}_p, \tau_p)$

$$(\mathbf{x}, \tau)_{(k+1)} = (\mathbf{x}, \tau)_{(k)} - [J(H_s(\mathbf{x}, \tau)_{(k)})]^{-1} H_s(\mathbf{x}, \tau)_{(k)}. \tag{18}$$

However, it is possible to identify in $H^{-1}(p, \tau)$ the roots found when the homotopic route path $\tau = 1$ using (17). In fact, the determination of the roots occurs in that place; although, it is challenging for the intersection of the homotopic path to occur precisely at that point. Therefore, in the vicinity of this value, when the step transitions from a lower number ($\tau_j < 1$) to a number greater than 1 ($\tau_{j+1} > 1$), the step prior to the find zero strategy (FZS, or refinement) of the roots is linear interpolation using the following formula:

$$\hat{\mathbf{x}} = \mathbf{x}_j + \frac{(\mathbf{x}_{j+1} - \mathbf{x}_j)}{(\tau_{j+1} - \tau_j)}(1 - \tau_j). \tag{19}$$

In order to generate the interpolated start points (ISPs) for FZS, the variables $\mathbf{x}_{j+1}$ and τ_{j+1} correspond to values when ($\tau > 1$), and $\mathbf{x}_j$, τ_j for ($\tau < 1$), $\mathbf{x}$ represents each of the variables, and $\hat{\mathbf{x}}$ are the interpolated values for each variable by setting $\tau = 1$ in the interpolation. The values found with (19) will be the ISP values for the N-R method in the FSZ procedure for $\tau = 1$, evaluated at $\hat{\mathbf{x}}$.

$$\mathbf{x}_{(k+1)} = \mathbf{x}_{(k)} - [J(f(\mathbf{x}_{(\mathbf{k})}))]^{-1} f(\mathbf{x}_{(k)}). \tag{20}$$

3.3 Flowchart and pseudocode

Figure 5 illustrates the flowchart of the algorithm for homotopy with hyperspherical tracking. Each of the key points of the algorithm is summarized as follows:

(1) The formulation of the system of homotopy equations is initiated by including the hypersphere equation.
(2) Set the number of iterations for hyperspheres and initialize the counter.

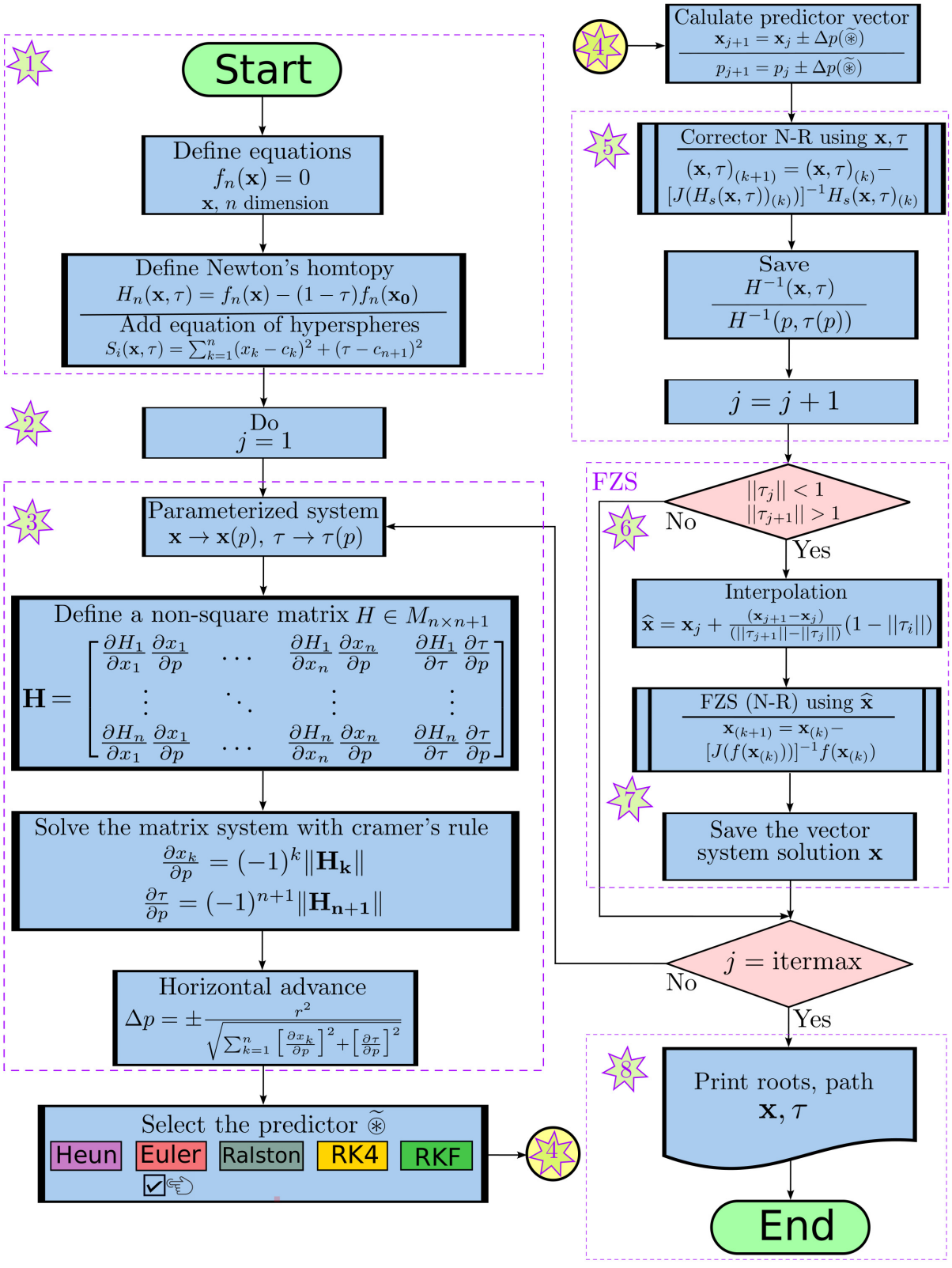

Figure 5: Flow chart for homotopy with hyperspherical tracking.

(3) Establish the nonsquare matrix $\mathbf{H}$. Calculate the determinants and multiply them by $(-1)^k$. Compute the horizontal advance Δp.
(4) Proceed to calculate the predictor vector. The symbol $\tilde{\circledast}$ refers to the chosen predictor. In this work, the Euler predictor, equation (15).
(5) Apply N-R for homotopic correction. Save in a list $H^{-1}(\mathbf{x}, \tau)$ and $H^{-1}(p, \tau(p))$. Update the counter.
(6) Calculate $\|\tau_j\|$ and $\|\tau_{j+1}\|$ for the FSZ strategy.
(7) Interpolate and apply N-R. Save the solutions in a list.
(8) If the number of hypersphere iterations has been reached, print the solutions and the homotopic tracking.

Note in the flow diagram that a predictor other than Euler's can be chosen, such as the Heun, Runge-Kutta, and fourth-order Runge-Kutta predictors, and Ralston [106,107]. In this work, the Euler predictor was implemented. **Algorithm 1** shows the pseudocode of the flowchart in Figure 5, where each necessary step for coding in programming languages such as Maple, Matlab, C++, Python, among others, is detailed. The presented pseudocode describes the implementation of the homotopy algorithm for hyperspherical tracking in a simplified manner, highlighting the main steps for its coding.
Algorithm 2 shows the pseudocode for the corrector_N-R subroutine of the flowchart in Figure 5. The subroutine receives as arguments the symbolic $J(H_s(\mathbf{x},\boldsymbol{\tau}))$, the vector $\mathbf{x}_p$, τ. Likewise, Algorithm 2 shows FSZ strategy N-R, FSZ_N-R. This subroutine receives, $\hat{\mathbf{x}}$, and symbolic $J(f(\mathbf{x}_k))$.

Algorithm 1: General Procedure for homotopy with hyperspherical tracking

```
Initialization blocks:
Step 1. Define τ = 0, x_0, itermax, TOL, r, n
Step 2. Defines the system of equations f(x) = 0
Step 3. Define system matriz and Jacobian, f(x), J(f(x))
Step 4. Formulation of the homotopy H_i(f(x), τ) = 0
Step 5. Add equation of hyperspheres S(x, τ) = 0
Step 6. Define matrix H ∈ M_{n×n+1} , and  J(H_s(x, τ))
Step 7. Loop for hyperspheres. Set a loop with j=1 and itermax
// Loop for hyperspheres //
for (j = 1; j =itermax; j = j + 1) do
    Step 8. Obtain the matrices from the Jacobian for the determinants
    Step 9. Calculate the determinants and multiply by (−1)^N
    for (N = 1; j =Ndet; N = N + 1) do
        Step 9a. Calculate ∂x_k/∂p see Eq.(13)
        Step 9b. Calculate ẏ_k see Eq.(14)
    Step 10. Calculate horizontal advance Δp, see Eq.(16)
    Step 11. Calculate predictor vector (In our case, ⊛̃ refers to Euler predictor), with Eq.(15) and ẏ_k
    Step 12. Calculate the corresponding point p to the horizontal adanvance, see Eq.(17)
    // Subroutine for corrector is Corrector_NR //
    Step 13. Call Corrector_NR (x_p, τ, J(H_s(x, τ))).
    Step 14. Save in a list or array and file text x, τ
    Step 15. Calculate the module ||τ||
    Step 16. FZS strategy. Check intersections of the homotopic path with ||τ|| = 1
    // Find zero strategy //
    if (||τ_j|| < 1  and ||τ_{j+1}|| > 1) then
        {
          Step 16a. Interpolate for x̂_i using Eq.(20) employing x_j, x_{j+1}, ||τ_j||, ||τ_{j+1}||, ||τ|| = 1
        // Subroutine for fZS is FZS_N-R //
        Step 16b. Call FSZ_NR (x̂, J(f(x))).
          Step 16c. Saves the homotopic tracking in a text file for plotting
        }
    else
        {
        Step 16d. Go to step 7
        }
Step 17. Print roots x, τ, H^{-1}
End program
```

Algorithm 2: Subroutines with N-R for corrector and FSZ

```
// Subroutine for Corrector_NR //
Corrector_NR ((x_p, τ, J(H_s(x, τ))).
Maximum number of iterations N
for (j = 1; j = N; j = j + 1) do
    //J(H_s(x, τ)) is evaluated in (x, τ)_(k) = (x_p, τ_p)
    //H_s(x, τ) is a vector, H evaluated in (x, τ)_(k) = (x_p, τ_p)
    (x, τ)_(k+1) = (x, τ)_(k) − [J(H_s(x, τ)_(k))]^(−1) H_s(x, τ)_(k)
    (x, τ)_(k) = (x, τ)_(k+1)
    if (||(x, τ)_(k+1) − (x, τ)_(k)|| < TOL then
        {
        return (x, τ)_(k)
        }
    else
        {
        print("Maximum number of iterations excedeed")
        }
End subroutine

// Subroutine for FSZ_NR //
FSZ_NR ((x̂, J(f(x))).
Maximum number of iterations N
for (j = 1; j = N; j = j + 1) do
    //J^(−1)(f(x)) is evaluated in x_(k) = x̂
    //f(x), equations system evaluated in x_(k) = x̂
    x_(k+1) = x_(k) − [J(f(x_(k)))]^(−1) f(x_(k))
    x_(k) = x_(k+1)
    if (||x_(k+1) − x_(k)|| < TOL then
        {
        return x_(k)
        }
    else
        {
        print("Maximum number of iterations exceeded")
        }
End subroutine
```

4 Case studies

The mesh analyses presented in the case studies are fundamental in the analysis of circuits within electrical and electronic engineering. Both mesh and node analyses are important in the analysis of electrical circuits [28]. In electrical engineering, the relevance of mesh analysis is vast, being applied, for example, in three-phase circuits and those involving motors [28]. Furthermore, in the analysis of AC circuits, the frequencies of the voltage sources generate reactances in components such as capacitors and inductors. With passive devices such as capacitors and inductors, we obtain impedance, whose unit of measurement is the ohm [15,28,31].

Likewise, these analyses allow the application of various theorems, such as Thevenin's theorem and the superposition theorem, among others, to simplify circuit analysis. In electronics, mesh analysis is essential for studying circuits with transistors, in both direct current and small signal analyses [108,109]. Transistors are the foundation of electronics and the design of analog integrated circuits, as well as integrated circuits of the transistor-transistor logic (TTL) and complementary metal-oxide-semiconductor (CMOS) families [108–110], microcontrollers [111], microprocessors [112], and others.

This section presents five case studies. The first involves a system of two algebraic simultaneous equations with real coefficients. The second and third case studies focus on mesh analysis of AC electrical circuits. In the fourth case study, the voltages of a small power system connected to a motor are determined. The final case study presents a mesh analysis of AC electrical circuits incorporating nonlinear impedances. In all case studies, we use the notation "*j*" for the imaginary part of the complex numbers, and the radius of the hyperspheres is $r = 0.003$. The convention for representing AC is to use the lowercase letter "**i**" in bold, as it denotes a complex quantity [15,28].

4.1 Case study 1

Solve the system of equations given by

$$\begin{aligned} x^3 - y + 1 &= 0, \\ \frac{1}{2}x - y - 1 &= 0. \end{aligned} \tag{21}$$

This system of equations can be solved by algebraic or numerical methods. To solve it, in this work, two SPs were proposed to solve the system (21), $\mathbf{P_1}(\mathbf{x}, \mathbf{y}) = \{0.0001 + 0.0j, -0.1 + j\}$ and $\mathbf{P_2} = \{0.59 + 0.59j, -1 + 0.01j\}$. Figure 6 displays the graphs of the system (21), where the real root is clearly observed.

Table 1 summarizes the roots found with SPs used, the direction of the tracking, right (R) and left (L), the hypersphere iterations used, and CPU time in seconds. For example, the solutions S_1 and S_2 were found using SP P_1, the first one with tracking R, and the second one with tracking L, using 49 hyperspheres. It is noteworthy that the magnitude of the imaginary part of (S_1) is small, on the order of 1×10^{-106}, rendering it effectively real. Solution S_3 was found using SP P_2 with L tracking using 17 hyperspheres, and S_2 was found again during R tracking using 29 hyperspheres. The hypersphere radius used was equal to 0.003. The convention employed in Table 1 of this case study remains consistent across other case studies where the revealed solutions are displayed.

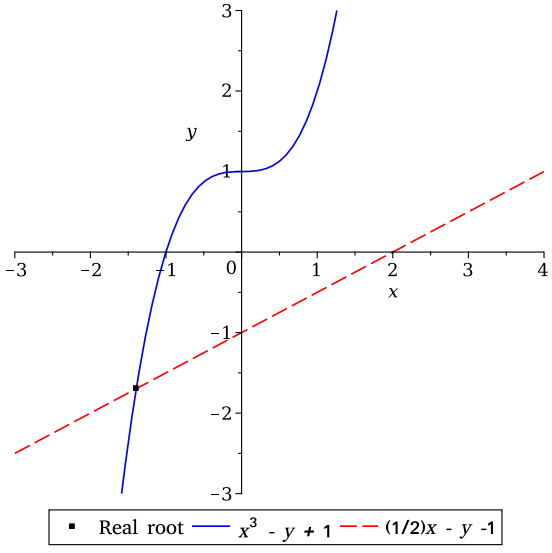

Figure 6: Plots for equations for case study 1.

Table 1: Homotopic tracking for case study 1

	Solution $S(\mathbf{x}, \mathbf{y})$	SP	Tracking	Hypersphere	Cpu-time [s]
$\mathbf{S_1}$	$-1.391768772235528 + 3. \times 10^{-388}j$ $-1.695884386117764 + 1. \times 10^{-388}j$	$\mathbf{P_1}$	R	49	1.012
$\mathbf{S_2}$	$0.6958843861177640 - 0.9760969401281266j$ $-0.6520578069411180 - 0.4880484700640633j$		L	49	1.019
$\mathbf{S_2}$		$\mathbf{P_2}$	R	29	0.671
$\mathbf{S_3}$	$0.6958843861177640 + 0.9760969401281266j$ $-0.6520578069411181 + 0.4880484700640633j$		L	17	0.431

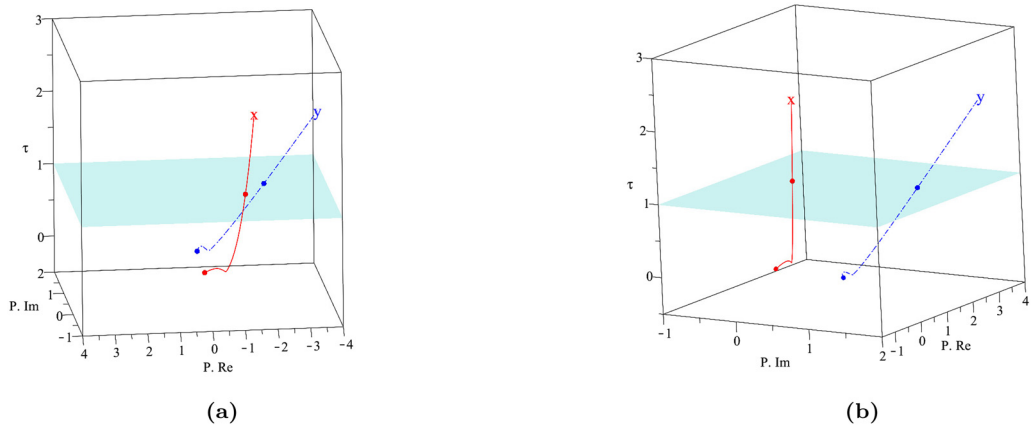

Figure 7: Hyperspheric homotopic tracking with $\mathbf{P_1}$ for case study 1. (a) Right tracking and (b) left tracking.

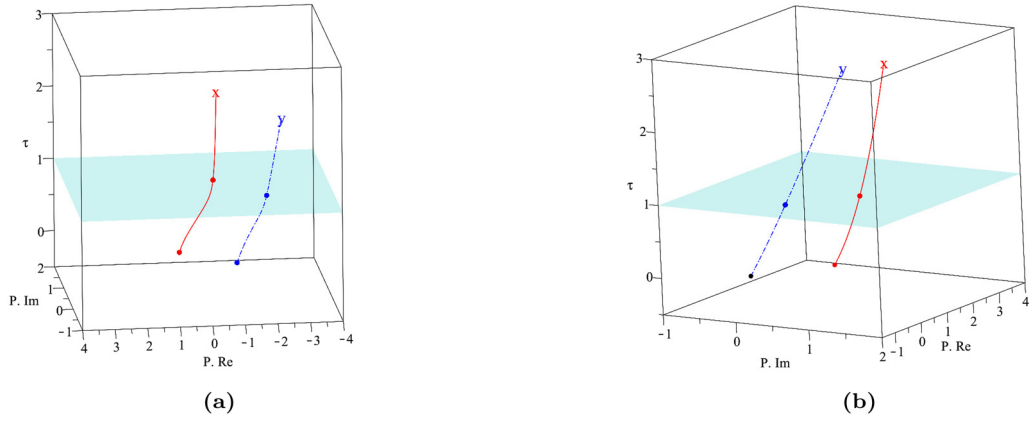

Figure 8: Hyperspheric homotopic tracking with $\mathbf{P_2}$ for case study 1. (a) Right tracking and (b) left tracking.

Figure 7 displays the homotopic tracking to find $\mathbf{S_1}$ and $\mathbf{S_2}$ for SP $\mathbf{P_1}$, and Figure 8 shows the homotopic tracking for SP $\mathbf{P_2}$ to find $\mathbf{S_2}$ and $\mathbf{S_3}$. Note that the trace for x presents a greater curlicue due to it being the variable with the greatest exponent. Observe that the axes of the figures are τ, imaginary part, and real part, respectively. At the intersection of the tracking trajectories with the plane $\tau = 1$ are the solutions for x, y, marked with two small spheres.

4.2 Case study 2

Find the mesh currents of the polarization point $\mathbf{Q}$ for the electric circuit in Figure 9.

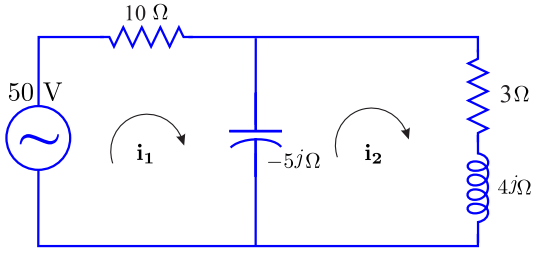

Figure 9: Electrical circuit with two meshes for case study 2.

This circuit was solved in [15] using Cramer's rule. The loop equations of the circuit in Figure 9 were formulated with Kirchhoff's law of charge conservation [15]. Therefore, the system of simultaneous equations of the circuit is given by

$$\begin{aligned}(10 - 5j)\mathbf{i_1} + (5j)\mathbf{i_2} - 50 = 0,\\ (5j)\mathbf{i_1} + (3 - j)\mathbf{i_2} = 0.\end{aligned} \tag{22}$$

Unlike the system of equations presented in case study 1, the coefficients of (22) in this case study are complex. Applying homotopy with hyperspherical tracking to solve the system of simultaneous equations, a SP $\mathbf{P}(\mathbf{i_1}, \mathbf{i_2}) = \{0.0001 + 0.01j, -0.1 + j\}$ [A] is employed. Table 2 shows the solutions and homotopic tracking carried out. In both tracking directions, the number of hyperspheres was 87. Similar times were obtained in both path tracking processes.

Figure 10 displays the homotopic tracking in both directions to determine solutions. Observe the linear behavior of the tracking paths for $\mathbf{i_1}$ and $\mathbf{i_2}$, which is characteristic of a linear system. In the plane $\tau = 1$, the solution is indicated with small spheres.

Table 2: Homotopic tracking for case study 2

Solution $Q(\mathbf{i_1}, \mathbf{i_2})$ [A]	SP	Tracking	Hypersphere	Cpu-time [s]
$2.80 + 0.4j$	$\mathbf{P}$	R	87	1.014
$2.0 - 4.0j$		L	87	1 009

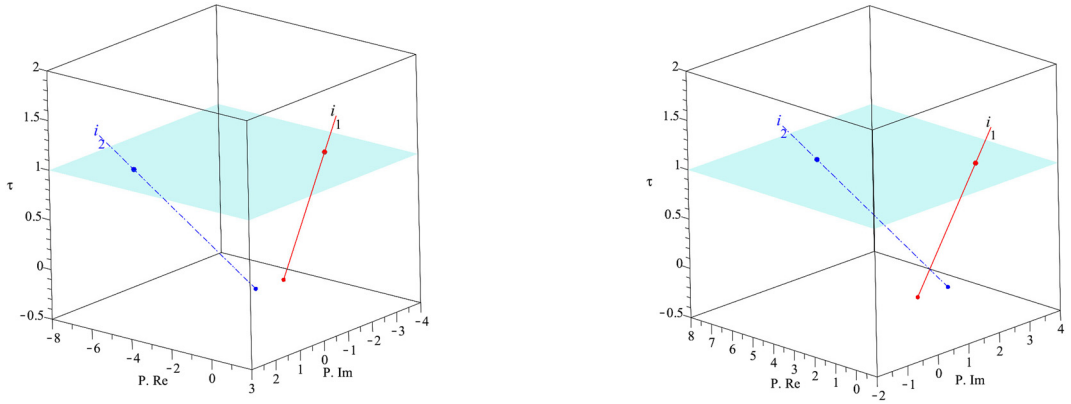

Figure 10: Hyperspheric homotopic tracking with $\mathbf{P}$ for case study 2. (a) Right tracking and (b) left tracking.

4.3 Case study 3

Find the mesh currents of the polarization point $\mathbf{Q}$ for the circuit in Figure 11.

Likewise, this circuit was solved in [15] using the rule of Cramer. The loop equations for the circuit in Figure 11 are given by

$$\begin{aligned}(5 + 5j)\mathbf{i_1} - (5j)\mathbf{i_2} - 30 = 0,\\ -5j\mathbf{i_1} + (8 + 8j)\mathbf{i_2} - 6\mathbf{i_3} = 0,\\ -6\mathbf{i_2} + 10\mathbf{i_3} + 20 = 0.\end{aligned} \tag{23}$$

Using the SP $\mathbf{P}(\mathbf{i_1}, \mathbf{i_2}, \mathbf{i_3}) = \{j, -1 + 0.02j, 1\}$ [A] for the homotopy, the mesh currents obtained are shown in Table 3.

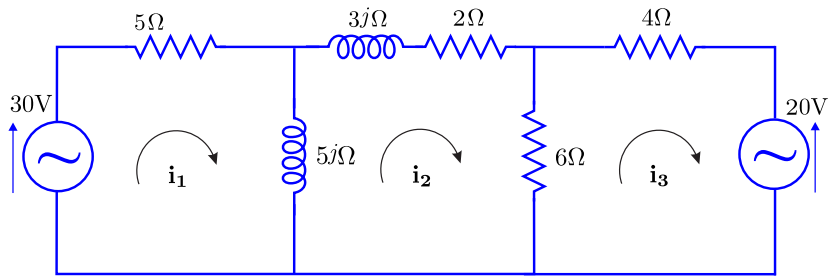

Figure 11: Electrical circuit with three meshes for case study 3.

Table 3: Homotopic tracking for case study 3

Solution $Q(\mathbf{i_1}, \mathbf{i_2}, \mathbf{i_3})$ [A]	SP	Tracking	Hypersphere	Cpu-Time [s]
$3.10403287952736 - 1.77857693295659j$		R	80	2.184
$1.32545594657077 + 1.11739018751605j$	**P**	L	80	2.207
$-1.20472643205754 + 0.670434112509633j$				

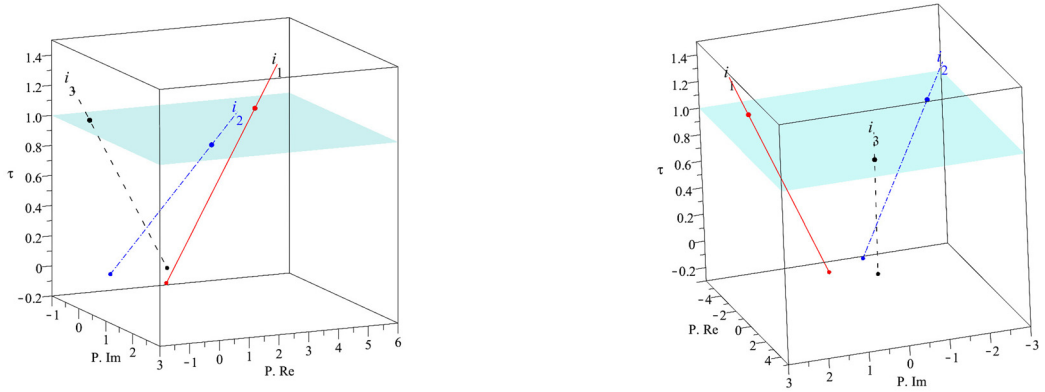

Figure 12: Hyperspheric homotopic tracking with **P** for case study 3. (a) Right tracking and (b) left tracking.

The behavior of the homotopic path exhibited by $\mathbf{i_1}$, $\mathbf{i_2}$, $\mathbf{i_3}$ is linear because the system of equations is linear. Figure 12 shows the homotopic tracking in both directions.

4.4 Case study 4

In [28], the problem for the single-line diagram of a small power system shown in Figure 13 (a) was solved. The equivalent reactance diagram, with reactances, is shown in Figure 13 (b). A generator with an electromotive force equal to 125 [V] per unit is connected through a transformer to high-voltage node 3, while a motor with internal voltage equal to $-0.481 - 0.481j$ [V] is connected to node 4. Figure 14 illustrates the circuit with the transformation of voltage generators into current sources, presenting the nodes to establish the nodal analysis equations. Determine all node voltages.

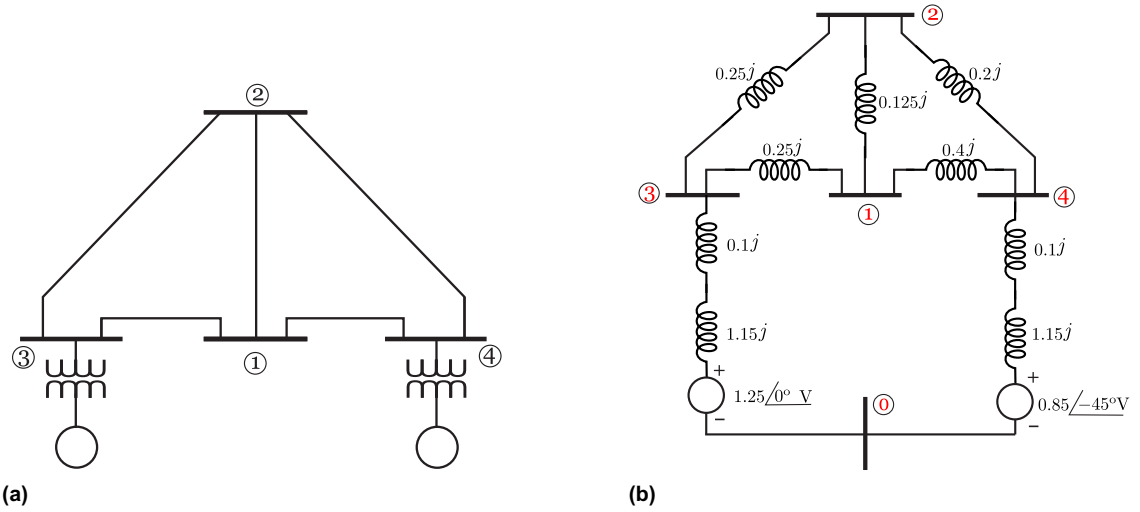

Figure 13: The single-line diagram of a small power system. (a) Single-line diagram of the four-bus system and (b) reactance diagram.

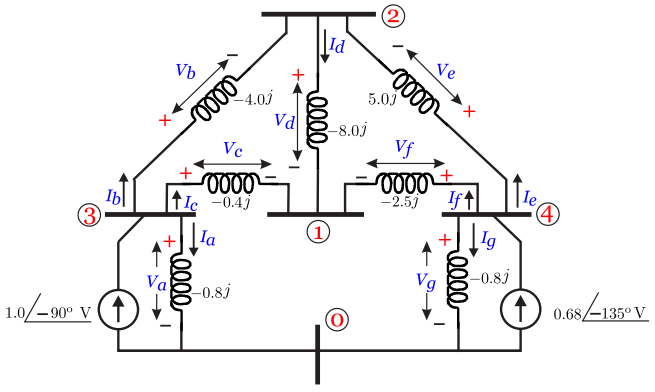

Figure 14: Electrical circuit with three meshes for case study 4.

Applying Kirchhoff's voltage law, the node voltage equations for the equivalent of Figure 14 is given by (24)

$$\begin{aligned}(-14.5j)\mathbf{v_1} + (8j)\mathbf{v_2} + (4j)\mathbf{v_3} + (2.5j)\mathbf{v_4} &= 0,\\ (8j)\mathbf{v_1} - (17j)\mathbf{v_2} + (4j)\mathbf{v_3} + (5j)\mathbf{v_4} &= 0,\\ (4j)\mathbf{v_1} + (4j)\mathbf{v_2} - (8.8)\mathbf{v_3} - j &= 0,\\ (2.5j)\mathbf{v_1} + (5j)\mathbf{v_2} - (8.3)\mathbf{v_3} - 0.481 - (0.481)j &= 0.\end{aligned} \tag{24}$$

Using the SP $\mathbf{P}(\mathbf{v_1}, \mathbf{v_2}, \mathbf{v_3}, \mathbf{v_4}) = \{0.5j, 0.1, 0.21, -0.4j\}$ [V] in the homotopy to solve (24), the node voltages are shown in Table 4. The operating point was obtained in both directions of hyperspherical tracking, utilizing 184 hyperspheres. Similar times were obtained in both path tracking processes.

Table 4: Homotopic tracking for case study 4

Solution $\mathbf{Q}(\mathbf{v_1}, \mathbf{v_2}, \mathbf{v_3}, \mathbf{v_4})$ [V]	Init point	Tracking	Hypersphere	Cpu-Time [s]
$0.9135231999999322 - 3.848182399999951j$		R	184	5.753
$0.5707647999999302 - 4.382633599999937j$	P	L	184	5.868
$3.741279999999949 + 0.5610399999999376j$				
$-2.514060800000087 - 9.192694399999815j$				

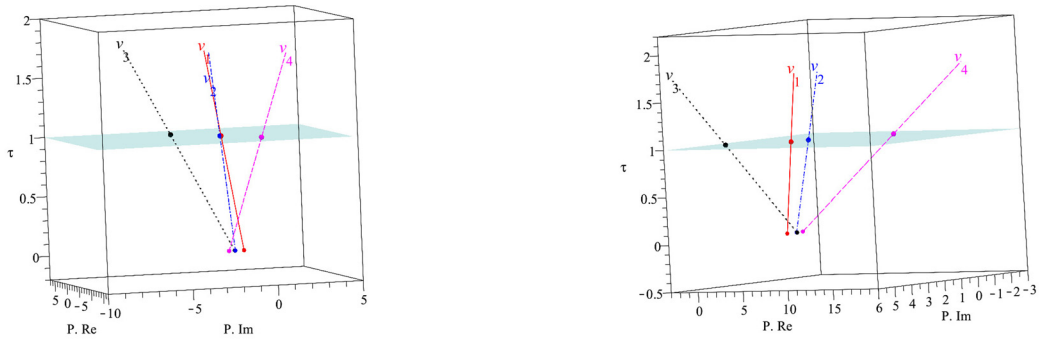

Figure 15: Hyperspheric homotopic tracking with **P** for case study 4. (a) Right tracking and (b) left tracking.

Figures 15 (a) and (b) display the hyperspherical homotopic tracking with linear behavior for each of the voltages of the system equation (24), showing the unique solution in the plane $\tau = 1$.

4.5 Case study 5

In [113], an electric circuit with a loop containing nonlinear elements was solved. In this case study, we will find the mesh currents for the electric circuit in Figure 16.

The formulas for nonlinear impedances [113,114] are given by

$$\begin{aligned} X_C &= \frac{1}{\omega C}\left(1 + \frac{3\gamma i^2}{2\omega^2}\right), \\ X_L &= \omega L\left(1 - \frac{3\beta i^2}{2}\right), \end{aligned} \tag{25}$$

where ω is the angular frequency in radians per second [rad/s], C is the capacitance in Farads [F], L is the inductance in Henrys [H], and the reactances X_C and X_L are given in (Ω) (Ohms). The coefficients γ and β are measures of nonlinearity and are positive in the absence of direct current polarization. Details on how these coefficients are determined are presented in [114].

For the mesh analysis of this problem, with nonlinear impedances in this case study, the following values are considered: $\gamma = 1.5\ [\text{rad}^2\ \text{C}^{-2}]$, $\beta = 1.5\ [\text{A}^{-2}]$, $\omega = 62.831$ [rad/s], $L_1 = 0.03$ [H], $C_1 = 0.0001$ F, $L_2 = 0.05$ H, and $C_2 = 0.0003$ [F]. Applying Kirchhoff's current law for each of the circuit meshes, three equations are obtained. By substituting the values for each one of the elements of the circuit and simplifying algebraically, we have a NAEs composed of three simultaneous equations.

$$\begin{aligned} (1.88495562j(1 - 2.250\mathbf{i}_1^2)\mathbf{i}_1 - 159.1549407j(1 + 0.000569931641\mathbf{1}\mathbf{i}_1^2) + 10)\mathbf{i}_1 - 10\mathbf{i}_2 - 5 = 0, \\ -10\mathbf{i}_1 + (24 + 18.9j(1 - 2.250\mathbf{i}_2^2))\mathbf{i}_2 - 5\mathbf{i}_3 = 0, \\ -5\mathbf{i}_2 + (11 - 53.051646913j(1 + 0.000569931641\mathbf{14}\mathbf{i}_3^2))\mathbf{i}_3 + 3 = 0. \end{aligned} \tag{26}$$

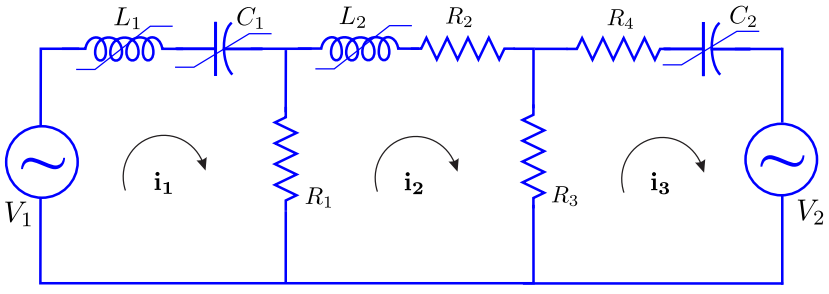

Figure 16: Electrical circuit with three meshes for case study 5.

To determine the operating points of the nonlinear circuit, two different SPs were proposed: $\mathbf{P_1}$ = {−5, −0.05j, −0.05j} [A] and $\mathbf{P_2}$ = {−10j, 0.05 − j, 0.05 − j} [A]. By using these SPs in the routine developed in this work, six operating points were found. Table 5 illustrates the six solutions of (26), along with the hyperspheric tracking. It is noteworthy that the operating point of the electric circuit $\mathbf{Q_1}$ was encountered twice during this tracking, specifically in hyperspheres number 40 and 287, respectively.

Figure 17 displays the homotopic tracking for the SP $\mathbf{P_1}$. In Figure 17(a), the homotopic tracking is presented to the right, where four operating points were found. In this manner, operating point $\mathbf{Q_1}$ is identified by the red sphere, $\mathbf{Q_2}$ by the blue sphere, $\mathbf{Q_3}$ by the gold sphere, and $\mathbf{Q_4}$ by the black sphere, all located in the plane τ = 1. It is important to note that hypersphere iterations 40 and 287 (for $\mathbf{Q_1}$) overlap because they represent the same root. Likewise, it should be observed that the homotopic path for $\mathbf{i_2}$ and $\mathbf{i_3}$ tends to form a loop since the trajectory does not change significantly. Figure 17(b) shows the tracking L, where only the operating point $\mathbf{Q_5}$ was found.

Table 5: Homotopic tracking for case study 5

	Solution $\mathbf{Q}(\mathbf{i_1}, \mathbf{i_2}, \mathbf{i_3})$[A]	SP	Tracking	Hypersphere	Cpu-Time [s]
$\mathbf{Q_1}$	$-3.404771613514471 - 0.06223348083020551j$ $-0.8290726033430187 - 0.2121534637067756j$ $-0.007605224851282848 - 0.1331113465575457j$	$\mathbf{P_1}$	R	40, 287	1.273 8.879
$\mathbf{Q_2}$	$0.001837586922971222 + 0.03129271558944998j$ $-0.0001454321064893533 + 0.001862317675217611j$ $-0.01141286269769539 - 0.05419605254377521j$			104	3.155
$\mathbf{Q_3}$	$0.02838479509310763 + 0.07669991807163615j$ $0.7482599714283836 - 0.3760137012274261j$ $0.03675550487009853 + 0.006352084290067902j$			132	3.979
$\mathbf{Q_4}$	$-3.414435858867392 - 0.09919531047346609j$ $1.040739135258746 - 0.5537424015900292j$ $0.05829553577252486 + 0.02945123417525128j$			196	5.853
$\mathbf{Q_5}$	$-3.385587352366261 - 0.07607010007611680j$ $-0.2116763603667693 + 0.7658393351317991j$ $-0.08441131285687606 - 0.05899582050942122j$		L	29	0.974
$\mathbf{Q_6}$	$1.747606204556523 - 2.859708356804453j$ $1.033635277443132 - 0.06194715752517483j$ $0.01372248294733972 + 0.03802389190396352j$	$\mathbf{P_2}$	L	57	1.461

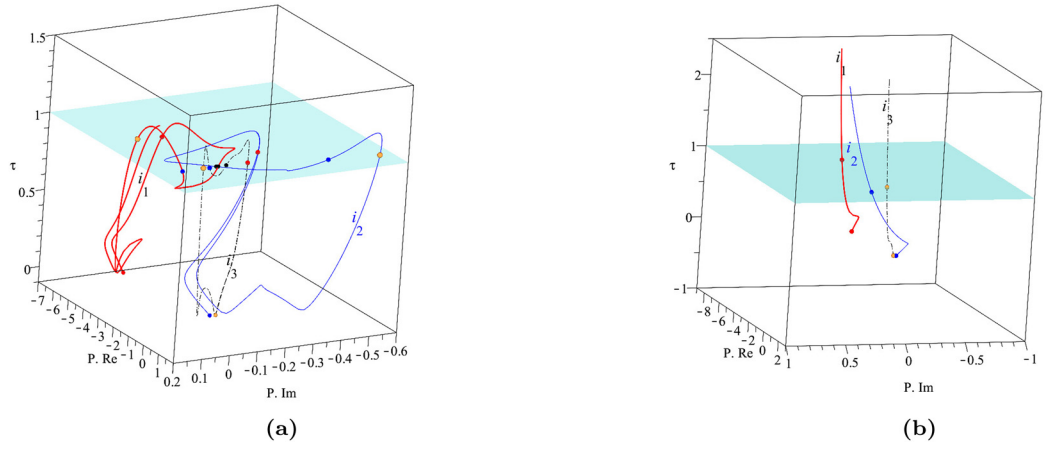

(a) (b)

Figure 17: Hyperspheric homotopic tracking with $\mathbf{P_1}$ for case study 5. (a) Right tracking and (b) left tracking.

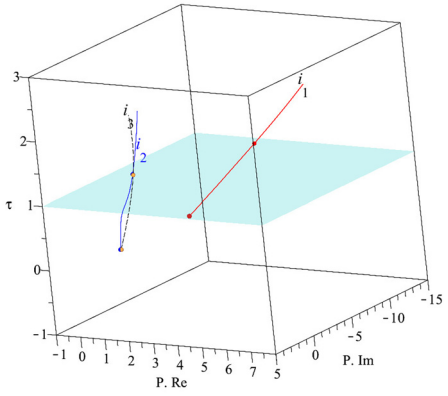

Figure 18: Hyperspheric homotopic tracking with $\mathbf{P}_2$ for case study 5.

Figure 18 presents the homotopic tracking on the left with SP $\mathbf{P_2}$ to find $\mathbf{Q}_6$. In general, in this case study, the homotopic tracking for all electrical intensities showed a nonlinear behavior.

5 Numerical simulation and discussion

The computer utilized for the development of this work was equipped with an Intel Core i7-7700U CPU @ 3.60 GHz with 4 cores and 8 threads, an NVIDIA Corporation GP107 [GeForce GTX 1050 Ti] graphics card, and 64 GB of RAM, operating on Linux Ubuntu version 20.04.6 LTS. For the implementation of the homotopy algorithm with hyperspherical tracking, Maple 2019 software was employed. In addition, in the simulations, the built-in Maple command, *fsolve*, was used to validate the results.

The analysis in this article focuses on identifying the complex roots of systems of algebraic equations, exploring the SDs found in the real and imaginary parts of each solution, as well as the iterations used. Tables 6–10 present the analysis of the SDs for the solutions of the case studies discussed in this article, utilizing the SPs provided by the linear interpolation of the homotopy algorithm. The criterion was to achieve more than ten SDs of accuracy in the solutions for the case studies. To validate the SD analysis, the SPs obtained from the interpolation (ISPs) were used in Maple's *fsolve* function with the respective system of equations for all case studies to obtain the exact solution with 15 SDs.

For case study 1, the real parts of all the solutions had 15 digits of accuracy. For $\mathbf{S_1}$, the imaginary part of its roots was of the order of 1×10^{-388}, so it was considered entirely a real solution. The root $\mathbf{S_2}$ was obtained with the two proposed SPs; it was the solution that required more iterations in its refinement. Similarly, when using

Table 6: Significant digits in the solutions for case study 1

Solution	ISP $(\widehat{\mathbf{x}}, \widehat{\mathbf{y}})$	Tracking	SD. Re	SD. Im	Iterations	Cpu-Time [ms]
$\mathbf{S_1}$	$-1.361815385844436 - 7.7503631085 \times 10^{-6}j$	R	15	388♠	5	24.1
	$-1.680907692922221 - 3.8751815485 \times 10^{-6}j$		15	388♠		
$\mathbf{S_2}$	$0.6393730848725269 - 0.2237879989427973j$	L	15	15	10	35.0
	$-0.680313457563745 - 0.111893999471449j$		15	15		
$\mathbf{S_2}$	$0.0927239123914071 - 0.7324583711010703j$	R	15	15	7	29.0
	$-0.9536380438042911 - 0.3662291855505289j$		15	14		
$\mathbf{S_3}$	$0.6948044564234470 + 0.9722854652888832j$	L	15	15	3	21.3
	$-0.6525977717882762 + 0.4861427326444419j$		15	15		

♠ The imaginary part is of the order of 1×10^{-388}, so there are 388 SD.

Table 7: Significant digits in the solutions for case study 2

Solution	ISP $(\widehat{\mathbf{i_1}}, \widehat{\mathbf{i_2}})$	Tracking	SD. Re	SD. Im.	Iterations	Cpu-Time [ms]
$\mathbf{Q}$	$2.80000000000008 + 0.399999999999914j$	R	Exact	Exact	1	29.1
	$2.00000000000001 - 4.00000000000023j$		Exact	Exact		
$\mathbf{Q}$	$2.80000000000003 + 0.399999999999985j$	L	Exact	Exact	1	28.4
	$2.00000000000000 - 3.99999999999998j$		Exact	Exact		

Table 8: Significant digits in the solutions for case study 3

Solution	ISP $(\widehat{\mathbf{i_1}}, \widehat{\mathbf{i_2}}, \widehat{\mathbf{i_3}})$	Tracking	SD. Re	SD. Im	Iterations	Cpu-Time [ms]
$\mathbf{Q}$	$3.104032879527390 - 1.778576932956540j$	R	15	15	1	31.1
	$1.325455946570853 + 1.117390187516078j$		15	15		
	$-1.204726432057508 + 0.6704341125096554j$		15	15		
$\mathbf{Q}$	$3.104032879527271 - 1.778576932956851j$	L	15	15	1	30.7
	$1.325455946570412 + 1.117390187515691j$		15	15		
	$-1.204726432057814 + 0.6704341125092399j$		15	14		

Table 9: Significant digits in the solutions for case study 4

Solution	ISP $(\widehat{\mathbf{v_1}}, \widehat{\mathbf{v_2}}, \widehat{\mathbf{v_3}}, \widehat{\mathbf{v_4}})$	Tracking	SD. Re	SD. Im	Iteration	Cpu-Time [ms]
$\mathbf{Q}$	$0.913523199999514 - 3.848182400008432j$	R	7	7	5	44.1
	$0.570764799998284 - 4.382633600009435j$		7	8		
	$3.741280000008137 + 0.561039999999007j$		6	5		
	$-2.514060800010422 - 9.192694400018024j$		**7**	8		
$\mathbf{Q}$	$0.913523200009666 - 3.848182400009999j$	L	7	7	1	35.9
	$0.570764800009906 - 4.382633600012517j$		7	8		
	$3.741280000010250 + 0.561040000008914j$		6	5		
	$-2.514060799990604 - 9.192694400033765j$		**7**	8		

The bold values are the interpolated values for each variable, as defined in equation (19).

$\mathbf{P_2}$, the imaginary part of y in $\mathbf{S_2}$ had 14 SDs of accuracy. Moreover, the solution $\mathbf{S_3}$ was the root that required the fewest iterations in its refinement.

For case study 2, the analysis of SD was precise. The algebraically obtained solutions for case study 2 are $\mathbf{i_1} = \frac{15}{4} + \frac{2}{5}j$ [A], $\mathbf{i_2} = 2 + 4j$ [A], while Table 2 presents their decimal equivalents. Table 7 demonstrates that accuracy was achieved in the first iteration in both directions of hyperspherical tracking. It is noteworthy that the SPs obtained through interpolation showed high accuracy, with some being identical to the refined solution values.

For case study 3, Table 8 shows high accuracy in the SD of all the electric currents obtained in the first refinement iteration for the electric circuit depicted in Figure 11. Only 14 SDs were achieved in the imaginary part of $\mathbf{i_3}$ in the homotopic tracking to the left.

For case study 4, the SDs obtained in the nodal voltages $\mathbf{v_1}, \ldots, \mathbf{v_4}$ using Maple's *fsolve* function did not reach 15 because the exact numerical solution was achieved. Table 9 illustrates this fact. For the root $\mathbf{v_4}$, seven SDs were obtained in their real part compared to the eight of the exact numerical solution. This result is highlighted in bold font within the table. It is noteworthy that in the left homotopic trace, only one iteration was required for refinement.

Table 10 likewise demonstrates high accuracy in the SDs of the operating points for the electric circuit in case study 5. There is at least 14 SD in the real parts of the solutions, while the imaginary parts achieve 13 SD,

Table 10: Significant digits in the solutions for case study 5

Solution	ISP $(\widehat{\mathbf{i_1}}, \widehat{\mathbf{i_2}}, \widehat{\mathbf{i_3}})$	Tracking	SD. Re	SD. Im.	Iterations	Cpu-time [ms]
$\mathbf{Q_1}$	$-3.402916988463000 - 0.06348596716694147j$	R	15	15	3	77.3
	$-0.8288297478016205 - 0.2121148710294159j$		15	15		
	$-0.007604161752556212 - 0.1330886777244804j$		14	15		
$\mathbf{Q_2}$	$0.00187524248267921 + 0.03124827751330032j$		15	15	2	73.1
	$-0.00022021871081716 + 0.001899903689216386j$		14	15		
	$-0.01141766065788088 - 0.05420210540081441j$		15	14		
$\mathbf{Q_3}$	$0.02837915640146923 + 0.07668407005611413j$		14	14	2	73.1
	$0.7483075953380905 - 0.3758397809714365j$		14	14		
	$0.03674068121858758 + 0.006359646316388135j$		14	13		
$\mathbf{Q_4}$	$-3.395649367270241 - 0.09627230926923084j$		15	14	3	77.0
	$1.039545795852312 - 0.5531820574082800j$		15	15		
	$0.05822254259902427 + 0.02935390021043543j$		15	15		
$\mathbf{Q_1}$	$-3.397822328184562 - 0.06337902155467005j$		15	15	3	77.2
	$-0.8284208846132136 - 0.2117305705501446j$		15	15		
	$-0.007631228052731898 - 0.1330445298327095j$		14	15		
$\mathbf{Q_5}$	$-4.543960062590368 + 0.02578042714209970j$	L	15	15	11	111.8
	$0.4023196303752304 - 0.2787420419366754j$		15	15		
	$0.02148418697380568 - 0.02308576418055790j$		15	15		
$\mathbf{Q_6}$	$1.888082121417342 - 7.612836953587082j$	L	14	14	8	99 2
	$0.7837877379774610 + 0.3318726817087686j$		14	14		
	$-0.027263802193360 0 + 0.0214038716627438j$		14	14		

as seen with $\mathbf{i_3}$ for $\mathbf{Q_3}$. The number of iterations required to refine the solutions $\mathbf{Q_1}$,..., $\mathbf{Q_4}$ ranged between 2 and 3. The ISPs provided by the interpolation also exhibited high accuracy. Nonetheless, the repetition of $\mathbf{Q_1}$ necessitated 11 iterations for its refinement, ultimately achieving 15 SD of accuracy in $\boldsymbol{i}_1$, $\boldsymbol{i}_2$, $\boldsymbol{i}_3$.

It is possible to determine the relative errors of all solutions presented in Tables 6–10 by employing the formula that associates the relative error with SDs [115,116], given by

$$\mathrm{SD} = -\log_{10}\left|\frac{v_A - v_E}{v_E}\right|, \tag{27}$$

where SD is the SDs, v_A is the approximate (measured) value, and v_E is the exact value.

Continuation homotopy with hyperspherical tracking can also experience numerical errors, similar to any numerical algorithm, such as round-off errors due to the finite precision of floating-point arithmetic in computers, numerical errors caused by nearly identical equations, convergence failure in N-R, or numerical instabilities [106,107]. These errors can cause the algorithm to lose homotopy path tracking. Furthermore, a study on the sensitivity of the algorithm indicates that it is generally more sensitive to the complexity of $f(\mathbf{x})$ than to its dimension, as reported in [117]. Table 11 presents a comparison of the computing times for $[J(H_s(\mathbf{x}, \tau))]^{-1}$ and $H^{-1}(\mathbf{x}, \tau)$ across all the case studies discussed in this work. The table includes the dimension $n + 1$ because the homotopy parameter τ was added to the system of equations to generate the homotopy. For instance, case studies 3 and 5 involve systems with three equations; however, it can be observed that the evaluation time for $[J(H_s(\mathbf{x}, \tau))]^{-1}$ is greater in the latter case. In addition, it is important to note that the CPU times for cases 4 and 5 are nearly identical. The comparison of computing times for all case studies was carried out using 300 hyperspheres with a radius of $r = 0.003$.

Table 12 presents a comparison of the computation times using differential path tracking and hyperspherical path tracking [34,39] for all the case studies analyzed in this work. The computation times obtained with hyperspherical path tracking are consistently shorter compared to those obtained with differential path tracking across all case studies. In addition, the number of iterations required in this study is lower when using hyperspherical path tracking compared to differential path tracking. It is noteworthy that in all case studies, all solutions were successfully found using hyperspherical path tracking, while differential path tracking only managed to identify some of them.

Table 11: CPU time for case $[J(H_s(\mathbf{x},\tau))]^{-1}$ and $H^{-1}(\mathbf{x},\tau)$

Study case	Cpu-Time for $[J(H_s(\mathbf{x},\tau))]^{-1}$ [ms]	Cpu-Time for $H^{-1}(\mathbf{x},\tau)$ [s]	Dimension $n+1$
1	21.20	R 5.649 L 5.604	3×3
2	25.82	R 4.476 L 3.486	3×3
3	33.42	R 7.896 L 7.958	4×4
4	41.02	R 9.646 L 9.369	5×5
5	55.34	R 9.086 L 9.025	4×4

Furthermore, it is important to note that the inclusion of complex numbers in hyperspherical tracking significantly increases computation times, in contrast to those reported in the literature when real numbers are employed.

Table 13 presents a comparison of solutions obtained using homotopy with hyperspherical path tracking and the Super Ostrowski homotopy continuation method (SOHCM) [118,119]. The table displays the solutions found with Super-Ostrowski HCM in the path tracking, except in case study 4. In general, the CPU times with SOHCM are shorter than this work. However, in some cases, the SP leads to finding a different root. For instance, in this work, solution S_1 was obtained with P_1 using the hyperspherical path tracking, whereas S_3 was found with SOHCM after 280 iterations.

For case study 5, using SOHCM, Q_5 was obtained with P_1, while employing homotopy with hyperspherical path tracking, the roots were identified in the order Q_1, Q_2, Q_3, Q_4, and Q_5. It is important to note that the iterations employed in SOHCM generally exceed 70 to achieve 15 SDs. However, in case study 5, 200 iterations were used to obtain 2 SD.

Likewise, the computational time increases as the complexity of the equation systems grows. Case study 5 requires a computational time of 4.005 [s] due to the system being nonlinear. In contrast, case study 4 does not

Table 12: Comparison for solutions using hyperspherical path tracking vs differential path tracking

Study case	Solution			This work		Differential path tracking	
	SP	Tracking		Iteration	Cpu-Time [s]	Iteration	Cpu-Time [s]
1	P_1	S_1	R	49	1.019	–	–
		S_2	L	49	1.012	124	1.522
	P_2	S_2	R	29	0.671	358	7.012
		S_3	L	17	0.431	357	6.464
2	P	Q	R	87	1.014	720	11.121
			L	87	1.009	690	7.350
3	P	Q	R	184	5.753	628	11.167
			L	184	5.868	627	12.054
4	P	Q	R	184	5.753	1972	52.017
			L	184	5.868	1972	50.024
5	P_1	Q_1	R	40	1.273	–	–
		Q_2	R	104	3.155	238	6.129
		Q_3	R	132	3.979	585	14.326
		Q_4	R	196	5.853	–	–
		Q_5	L	29	0.974	–	–
	P_2	Q_6	L	57	1.461	–	–

Table 13: Comparison for solutions using hyperspherical path tracking vs. super-Ostrowski HCM

Study case	SP	This work			Super-Ostrowski HCM		
		Tracking	Iteration	Cpu-Time [s]	Tracking	Iteration	Cpu-Time [s]
1	P_1	S_1 R	49	1.019	S_3 R	280	0.365
		S_2 L	49	1.012	–	–	–
	P_2	S_2 R	29	0.671	S_2 R	280	0.349
		S_3 L	17	0.431	–	–	–
2	P	Q R	87	1.014	Q R	25	0.018
		L	87	1.009	–	–	–
3	P	Q R	184	5.753	Q R	78	0.217
		L	184	5.868	–	–	–
4	P	Q R	184	5.753	Q R	⊗	–
		L	184	5.868	–	–	–
5	P_1	Q_1 R	40	1.273	–	–	–
		Q_2 R	104	3.155	–	–	–
		Q_3 R	132	3.979	–	–	–
		Q_4 R	196	5.853	–	–	–
		Q_5 L	29	0.974	Q_5 R	200	4.055
	P_2	Q_6 L	57	1.461	Q_6 R	200♦	0.333

⊗ Divergence.

♠ 2 SD were obtained.

have a solution. Furthermore, in [118], the structure of the homotopy includes a squared homotopic parameter, and the path tracking does not use any predictor, such as Euler, among others. However, it is possible to obtain τ with higher exponents if $G(x, \tau)$, as shown in equation (14) in [118], becomes more complicated. Actually, instead of that, SOHCM uses a simple proportional predictor. The algorithm requires the number of iterations to be set up *a priori*. The SOHCM algorithm uses the number of iterations as the denominator, with a counter in the numerator for this fraction. The solution is considered found when the numerator equals the denominator, resulting in $\tau = 1$. For this reason, Table 13 only shows right path tracking in SOHCM. Likewise, SOHCM can only find one solution when $\tau = 1$ because the algorithm terminates at $\tau = 1$. In this research, equation (14) from [118] was implemented with hyperspherical path tracking, using a hypersphere radius of 0.003; however, divergence was encountered. Nonlinear terms in the structure of any homotopy cause numerical instabilities in path tracking. The results presented in this study were obtained using an Euler predictor with path tracking in both directions.

The path tracking behavior in Figures 10, 12, and 15 for case studies 2, 3 and 5, respectively, exhibits a linear trend because the systems of equations in theses case studies are linear. In contrast, Figures 7 and 8 in case study 1 and Figures 17 and 18 in case study 5 display nonlinear behavior. As the nonlinearity in the system of equations increases, the homotopic tracking demonstrates a more pronounced nonlinear behavior, as seen in Figure 17. However, Figures 19 and 20 show the graph homotopic parameter τ versus advance parameter p used in hyperspherical path tracking. These figures highlight the advantage of utilizing the advance parameter p, as it facilitates the visualization of all solutions via homotopic path tracking. In addition, the graphs depict the system's behavior. For example, Figures 19 (b)–(d) exhibit linear behavior because the systems of equations are linear for case studies 2, 3, and 4. In contrast, Figures 19 (a) and 20 for case studies 1 and 5, respectively, reveal nonlinear homotopic path tracking, attributed to the nonlinearity of the systems of equations in these cases. It is important to note that Figures 19 and 20 are in good agreement with the figures for hyperspheric homotopic tracking shown in each case study. For instance, Figure 20 (a) shows significant nonlinear behavior in homotopic path tracking for six solutions (five solutions in right tracking, and one solution in left tracking), while Figure 17 (a) depicts nonlinear behavior for each solution.

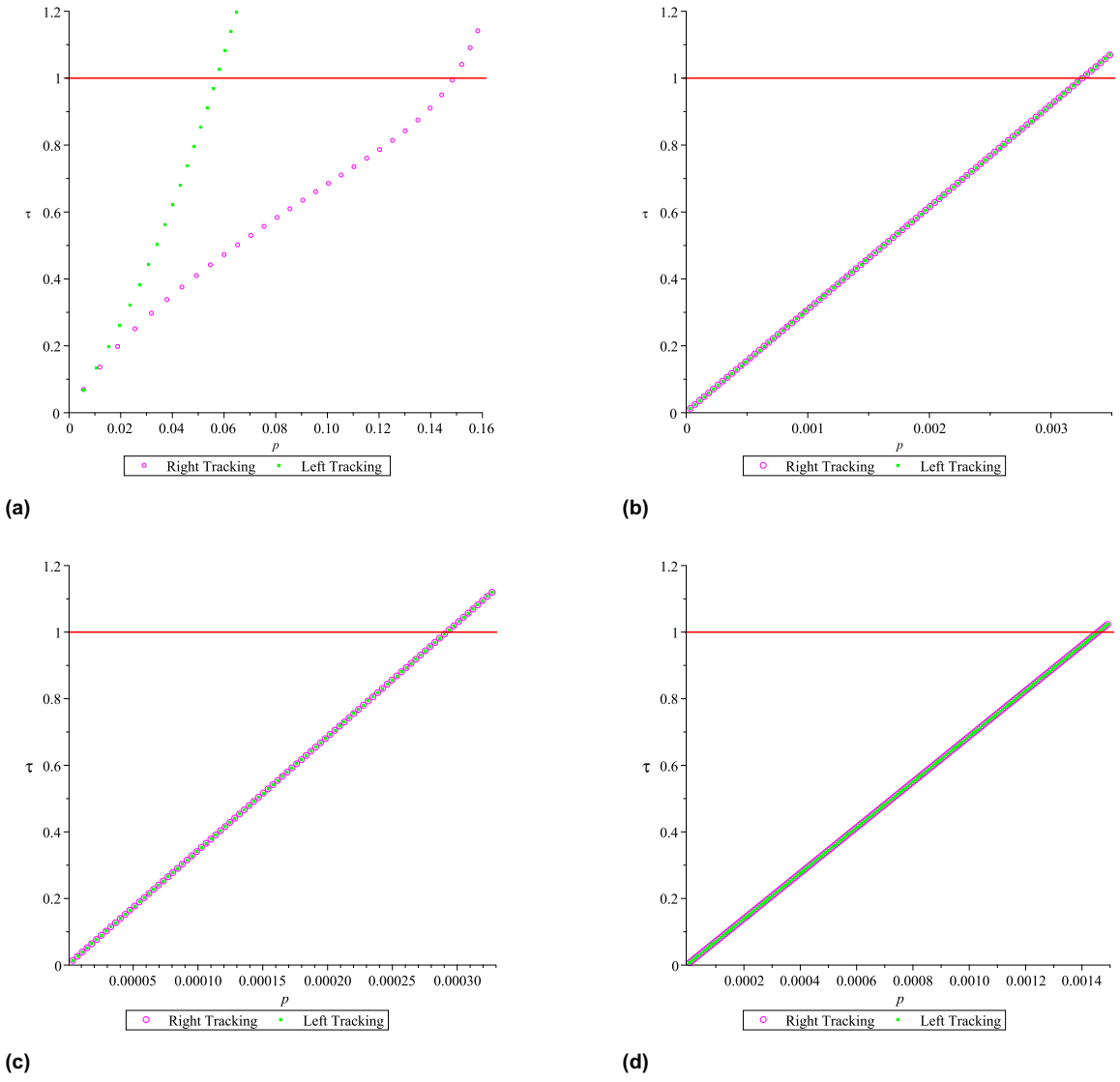

Figure 19: Homotopic advance p for case studies 1–4. (a) Homotopic tracking p vs τ for case study 1, (b) homotopic tracking p vs τ for case study 2, (c) homotopic tracking p vs τ for case study 3, and (d) homotopic tracking p vs τ for case study 4.

For SP P_2 in study case 5, Figure 20 (b) shows only left path tracking with its solution. It is important to note that the right tracking is not shown because a divergence occurred, and consequently, the solution cannot be determined.

Figure 21 shows the attractor basins for case study 1. Both figures were generated using the computer program Maple 21, with $\varepsilon = 1 \times 10^{-8}$. The attractor basin for N-R is defined as $A = [-2, 2] \times [-2, 2]$, and the attractor basin for Homotopy is $A = [-2.5, 2.5] \times [-2.5, 2.5]$. The step size used for all iterations is $k = 0.003$. The parameter ε indicates the accuracy of the calculated root, and A represents the area within which we draw the basins of attraction. The iterations and the colors used to draw the attraction basins in Figure 21 are listed in Table 14.

In the generated images, each point in the complex region that converges to a specific root is colored to match that root, with darker shades indicating a higher number of iterations and lighter shades fewer iterations. Points that do not converge within the iteration limit are colored gray. Figure 21 (a) shows the basins for a system with roots S_1, S_2, and S_3 using the N-R method, taking 50 min to generate, while Figure 21 required 29 h and 14 min. Convergence speed and dynamical behavior are reflected in the color shades and

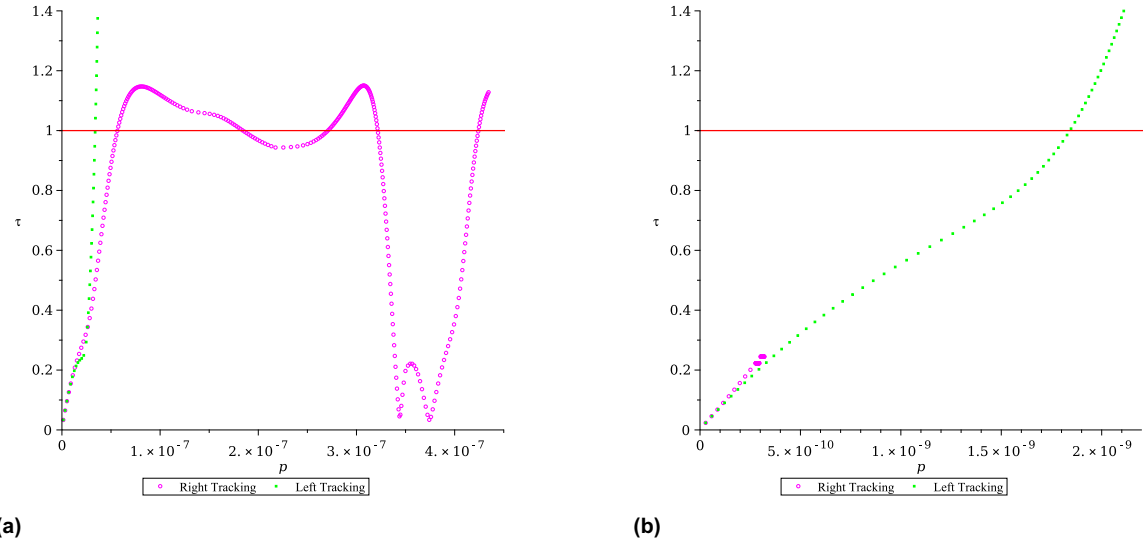

Figure 20: Homotopic advance p for case study 5. (a) Homotopic tracking p vs τ for P_1 and (b) left tracking p vs τ for P_2.

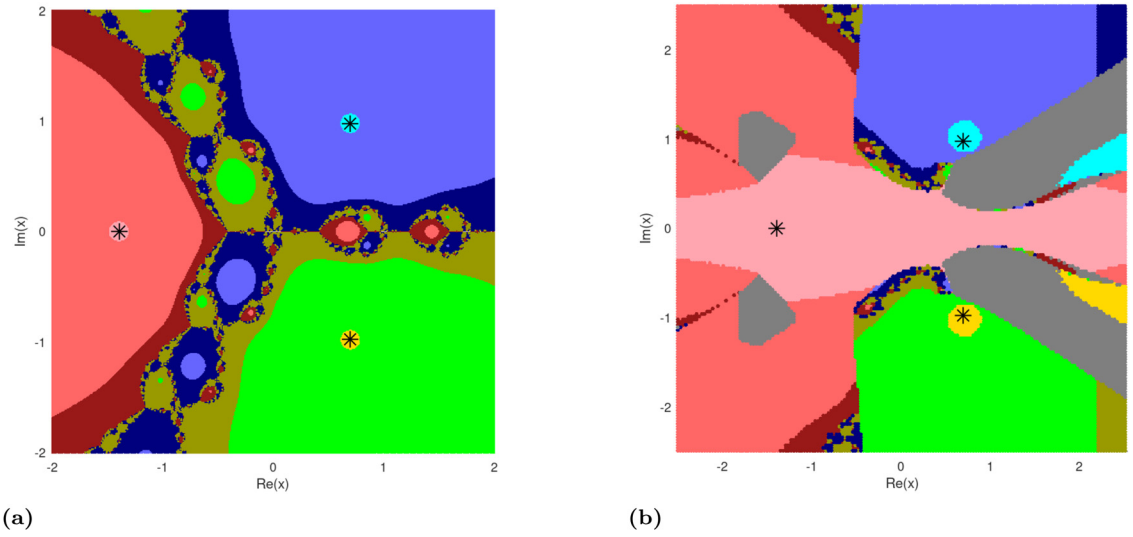

Figure 21: Basins of attractions for case study 1. (a) Newton basin and (b) homotopy basin.

variations, respectively, with uniform regions indicating consistent iteration counts, giving a contour-like appearance.

In the figure, stability occurs when the initial point is located within a basin of attraction that contains a root. Conversely, instability arises when the SP leads to a trajectory that exits the colored zone and diverges to a distant region, potentially converging to a different root. Moreover, the basin boundaries generated by the N-R method intersect, forming the Julia set, a complex boundary where chaotic behavior manifests. It is important to keep in mind that a complex analytical function divides the plane into two distinct regions: the Fatou set, a stable area characterized by relatively simple dynamics, and the Julia set [14,120–122], which forms the chaotic boundary of the Fatou set [120,122].

Figure 21 (b) displays the attraction basins for the homotopy method with hyperspherical path tracking for x, exhibiting noticeable symmetry at first glance. Since the basins for y are similar, only those for x are shown. However, significant differences can be observed when compared to the basins in Figure 21 (a). Specifically, the basin boundaries do not extend continuously from a common point. In addition, four regions appear

Table 14: Iterations in attraction basins for case study 1, Figure 21

Root	Iterations	Color code
S_1	$1-4$	
	$5-8$	
	$9-$	
S_2	$1-4$	
	$5-8$	
	$9-$	
S_3	$1-4$	
	$5-8$	
	$9-$	

where points fail to converge within the iteration limit; these regions are shown in gray, indicating divergence. Figure 21 (b) also exhibits chaotic behavior similar to Newton's basins when the initial point lies within the fractal structure. For instance, near the boundaries of the basins for S_1 and S_3, some SPs converge to S_2 in olive green. However, the basins also suggest a high degree of stability, as the areas in light colors are significantly larger compared to those in dark colors (up to 24 iterations were needed). Consequently, convergence occurs toward the root located within the respective basin.

6 Conclusions

This study introduced a comprehensive exploration of the HCM combined with hyperspherical tracking to identify complex roots in systems of equations with applications to electrical circuits. The research conducted spanned a variety of case studies, ranging from systems of algebraic equations to complex electrical circuits with nonlinear elements. The findings of this study emphasize the efficacy and precision of the HCM with hyperspherical tracking in solving complex systems of equations.

The case studies presented illustrate the method's capability to accurately determine complex roots, even in scenarios involving nonlinear elements and imaginary coefficients. The precision of the solutions was validated against existing literature and through the use of Maple's *fsolve* function, demonstrating the method's reliability and effectiveness. The analysis of SDs further underscored the method's high level of accuracy, with most solutions achieving close to or exactly the desired number of SDs.

In addition, the study of basins obtained through homotopy requires an in-depth analysis of their behavior, as well as an examination of the potential existence of Julia sets or other related structures. The basin of attraction obtained through continuation homotopy extends the analysis of these basins while also broadening the study of continuation methods using this technique. On the other hand, it remains to study the causes of divergence of the homotopy in the basin of attraction.

Notably, the study also highlighted the method's versatility in handling both linear and nonlinear systems, as well as its ability to find multiple operating points in electrical circuits. This versatility makes the HCM with hyperspherical tracking a valuable tool for researchers and practitioners in various fields, including electrical engineering, where complex systems of equations frequently arise.

Furthermore, the research presented contributes to the ongoing development of numerical methods for solving systems of equations. By demonstrating the practical applications of the HCM with hyperspherical tracking, this study adds to the body of knowledge and provides a foundation for future research in this area. The study proposes several avenues for future exploration. First, the homotopy routine with hyperspherical path tracking will be implemented in the C++ language using symbolic computation [123] to reduce computational time for tasks such as Jacobian computation, hyperspherical path tracking. Second, the application of homotopy with hyperspherical tracking is suggested to find complex roots of characteristic polynomials in systems theory. This method could aid in analyzing stability, frequency response, and other crucial aspects [29]. Third, there is a proposal to develop a routine for microcontrollers, aimed at facilitating educational research focused on implementing control systems that require real-time monitoring of stability, frequency

response, and other parameters. Moreover, the study suggests investigating the tracking of complex homotopic trajectories applied to robotics, particularly in navigating obstacles in the complex plane. This research could build upon previous works in the field [60,105]. Finally, it is proposed to explore in the future the possibility of using nonlinear interpolation [124–126] in FZS to reduce the number of iterations.

In conclusion, the HCM with hyperspherical tracking has proven to be a robust and precise approach for identifying complex roots in systems of equations. Its successful application to a diverse range of case studies underscores its potential as a numerical tool for solving complex problems in science and engineering. Future research could explore the method's applicability to other complex systems and further optimize its implementation for enhanced efficiency and accuracy.

Acknowledgements: The first author is currently research fellow at Tecnológico Nacional de México en Celaya. He expresses his gratitude for the support received.

Funding information: This research did not receive any specific grant from funding agencies in the public, commercial, or not-for-profit sectors.

Author contributions: MASH, HJI, HVL: conceived and designed the experiments; performed the experiments; Analyzed and interpreted the data; contributed reagents, materials, analysis tools or data; wrote the article. MLQV, MLLG: performed the experiments; analyzed and interpreted the data; contributed reagents, materials, analysis tools, or data.

Conflict of interest: Dr. Hector Vazquez-Leal is an Editor of the Open Mathematics journal and was not involved in the review and decision-making process of this article.

Data availability statement: All data analyzed during this study are included in this published article.

References

[1] F. Rivero-Mendoza, *Una introducción a los números complejos*, Editorial Universidad de los Andes, Mérida, Venezuela, 2001.
[2] H. Cardano, *Artis magnae, sive de regulis algebraicis, liber unus*, Franco Angeli, Milan, Italy, 2011.
[3] C. R. Maluendas, *Una breve historia imaginaria*, Univ. Nac. Colomb. **1** (2019), no. 2, 1–9. https://editorial.konradlorenz.edu.co/2019/02/paskin-matematico.html.
[4] R. Bombelli, *LaAlgebra*, Feltrinelli, Milan, Italy, 1966.
[5] R. Descartes, *La Géométrie*, A. Herman, Librairie Scientifique, París, 1637.
[6] B. Branner, *Caspar Wessel. On the Analytical Representation of Direction: An Attempt Applied Chiefly to Solving Plane and Spherical Polygons*, The Royal Danish Academy of Sciences and Letters, Copenhagen, Denmark, 1999.
[7] J. R. Argand, *Essai sur une manière de représenter les quantités imaginaires dans, les constructions géométriques*, Gauthier-Villars, Imprimeur-Libraire, Paris, France, 1874.
[8] L. Euleri, *Introductio in analysin infinitorum*, Tomus primus, Lausannae: apud Marcum-Michaelem Bousquet & Socies, Lausanne, Switzerland, 1748, http://hdl.handle.net/10481/31374.
[9] L. Euler, *Elements of Algebra*, Springer-Verlag, WI, USA, 1972.
[10] M. Hazewinkel, *Encyclopaedia of Mathematics*, Springer Science & Business Media, New York, USA, 1994.
[11] S. Gutiérrez, *Hamilton: La liberación del álgebra*, Suma **49** (2005), no. 49, 95–99. https://revistasuma.fespm.es/sites/revistasuma.fespm.es/IMG/pdf/49/095-099.pdf.
[12] J. M. Sánchez, *Historias de Matemáticas: Hamilton y el descubrimiento de los cuaterniones*, Pens. Mat. **1** (2011), no. 27. https://dialnet.unirioja.es/servlet/articulo?codigo=3744306.
[13] C. P. Steinmetz, *Complex Quatities and their use in electrical engineering*, Proc. Int. Electr. Congr. Am. Inst. Electr. Eng. August 21st to 25th American Institute of Electrical Engineers, USA, 1893, pp. 33–75.
[14] A. D. Wunsch, *Variable Compleja con Aplicaciones*, Pearson Educación, México, 1997.
[15] J. A. Edminister, *Circuitos Eléctricos, Serie Schaum*, McGraw-Hill, México, 1982.
[16] B. Mandelbrot, *The Fractal Geometry of Nature*, Free-man and Co., Mexico, 1977.
[17] C. Monroy-Olivares, *Curvas Fractales*, Alfaomega, México, 2002.

[18] M. J. Neve, *Reinterpreting the Smith chart using conformal geometric algebra*, IEEE Access **11** (2023), 138827–138838, DOI: https://doi.org/10.1109/ACCESS.2023.3340143.

[19] A. N. Kani, *Digital Signal Processing*, CBS Publishers and Distributors, New Delhi, India, 2022.

[20] G. A. Muñoz-Fernández and J. B. Seaone-Sepulveda, *Fundamentos y Problemas Resueltos de Teoría Cualitativa de Ecuaciones Diferenciales*, Ediciones Paraninfo, 2017.

[21] A. L. Granados, *Fractal techniques to measure the numerical instability of optimization methods*, Comput. Mech. **15** (1995), no. 9, 369–374.

[22] J. M. Gutiérrez, L. J. Hernández-Paricio, M. Marañón-Grandes, and M. T. Rivas-Rodríguez, *Influence of the multiplicity of the roots on the basins of attraction of Newton's method*, Numer. Algorithms **66** (2014), 431–455.

[23] J. M. Gutiérrez, *Numerical properties of different root-finding algorithms obtained for approximating continuous Newton's method*, Algorithms **8** (2015), no. 4, 1210–1218, DOI: https://doi.org/10.3390/a8041210.

[24] L. J. Hernández-Paricio, *Bivariate Newton-Raphson method and toroidal attraction basins*, Numer. Algorithms **71** (2016), 349–381, DOI: https://doi.org/10.1007/s11075-015-9996-3.

[25] M. Sandoval-Hernandez, H. Vazquez-Leal, L. Hernandez-Martinez, U. A. Filobello-Nino, V. M. Jimenez-Fernandez, A. L. Herrera-May, et al., *Approximation of Fresnel integrals with applications to diffraction problems*, Math. Probl. Eng. **2018** (2018), 4031793, DOI: https://doi.org/10.1155/2018/4031793.

[26] M. Maggiore, *A Modern Introduction to Classical Electrodynamics*, Oxford University Press, Oxford, UK, 2023.

[27] A. Cardama-Aznar, L. Jofre-Roca, J. M. Rius-Casals, J. Romeu-Robert, S. Blanch-Boris, and M. Ferrando-Bataller, *Antenas*, Univ. Politècnica de Catalunya, Alfaomega, Espannna, 2004.

[28] J. J. Grainger and W. D. Stevenson Jr, *Power System Analysis*, McGraw-Hill Series in Electrical and Computer Engineering, Singapore, 1994.

[29] K. Ogata, *Ingeniería de Control Moderna*, Quinta edición, Pearson Educación, México, 2010.

[30] T. Deliyannis, Y. Sun, and J. K. Fidler, *Continuous-time Active Filter Design*, CRC Press, Boca Raton, Florida, USA, 2020.

[31] L. P. Huelsman, *Active and Passive Analog Filter Design: An Introduction*, McGraw Hill, New York, 1993.

[32] J. V. Uspensky, *Teoría de Ecuaciones*, Limusa, México, 1987.

[33] M. A. Jenkins and J. F. Traub, *Algorithm 419: zeros of a complex polynomial [C2]*, Commun. ACM, **15** (1972), no. 2, 97–99, DOI: https://doi.org/10.1145/361254.361262.

[34] M. A. Sandoval-Hernandez, O. Alvarez-Gasca, A. D. Contreras-Hernandez, J. E. Pretelin-Canela, B. E. Palma-Grayeb, V. M. Jimenez-Fernandez, et al., *Exploring the classic perturbation method for obtaining single and multiple solutions of nonlinear algebraic problems with application to microelectronic circuits*, Int. J. Eng. Res. Technol. **8** (2019), no. 9, 636–645. https://www.ijert.org/exploring-the-classic-perturbation-method-for-obtaining-single-and-multiple-solutions-of-nonlinear-algebraic-problems-with-application-to-microelectronic-circuits.

[35] F. Dubeau and C. Gnang, *Fixed point and Newton's methods in the complex plane*, J. Complex Anal. **2018** (2018), 1–11, DOI: https://doi.org/10.1155/2018/7289092.

[36] F. Çilingir, *Singular perturbations arising in complex Newton's method*, Hacet. J. Math. Stat. **52** (2023), no. 5, 1–7, DOI: https://doi.org/10.15672/hujms.1132257.

[37] M. Sandoval-Hernandez, H. Vazquez-Leal, U. Filobello-Nino, E. De-Leo-Baquero, A. C. Bielma-Perez, J. C. Vichi-Mendoza, et al., *The quadratic equation and its numerical roots*, Int. J. Eng. Res. Technol. **10** (2021), no. 6, 301–305. https://www.ijert.org/research/the-quadratic-equation-and-its-numerical-roots-IJERTV10IS060100.pdf.

[38] K. Gdawiec, I. K. Argyros, S. Qureshi, and A. Soomro, *An optimal homotopy continuation method: Convergence and visual analysis*, J. Comput. Sci. **74** (2023), 1–12, DOI: https://doi.org/10.1016/j.jocs.2023.102166.

[39] T. L. Wayburn and J. D. Seader, *Homotopy continuation methods for computer-aided process design*, Comput. Chem. Eng. **11** (1987), no. 1, 7–25, DOI: https://doi.org/10.1016/0098-1354(87)80002-9.

[40] J. Farhang, J. D. Seader, and S. Khaleghi, *Global solution approaches in equilibrium and stability analysis using homotopy continuation in the complex domain*, Comput. Chem. Eng. **32** (2008), no. 10, 2333–2345, DOI: https://doi.org/10.1016/j.compchemeng.2007.12.001.

[41] H. Vazquez-Leal, et al., *Biparameter homotopy-based direct current simulation of multistable circuits*, Br. J. Math. Comput. Sci. **2** (2012), no. 3, 137–150, https://journaljamcs.com/index.php/JAMCS/article/view/1240.

[42] M. D. L. L. López-González, M. L. Quemada-Villagómez, M. G. Martínez-González, J. M. Oliveros-Muñoz, and H. Jiménez-Islas, *A novel predictive homotopic path tracking algorithm to solve non-linear algebraic equations*, Can. J. Chem. Eng. **101** (2023), no. 6, 3382–3408, DOI: https://doi.org/10.1002/cjce.24694.

[43] J. R. White, *Case study: Protein folding using homotopy methods*, Scientific Computing with Case Studies, SIAM Press, Philadelphia, USA, 2009, pp. 1–8. https://www.cs.umd.edu/oleary/SCCS/supp/White/Homotopy_paper.pdf.

[44] H. Jimenez-Islas, *Sehpe: Programa para la solución de sistemas de ecuaciones no lineales mediante método homotópico con seguimiento hiperesférico*, Av. Ing. Quím. **6** (1996), no. 2, 174–179.

[45] J. M. Oliveros-Munoz and H. Jiménez-Islas, *Hyperspherical path tracking methodology as correction step in homotopic continuation methods*, Chem. Eng. Sci. **97** (2013), no. 28, 413–429, DOI: https://doi.org/10.1016/j.ces.2013.03.053.

[46] H. Jiménez-Islas, M. Calderón-Ramírez, G. M. Martínez-González, M. P. Calderón-Álvarado, and J. M. Oliveros-Munoz, *Multiple solutions for steady differential equations via hyperspherical path-tracking of homotopy curves*, Comput. Math. Appl. **78** (2020), no. 8, 2216–2239, DOI: https://doi.org/10.1016/j.camwa.2019.10.023.

[47] L. O. Chua, *Nonlinear Network Analysis-the Parametric Approach*, Ph.D. Thesis, University of Illinois, June 1964. https://hdl.handle.net/2142/74281.
[48] L. O., Chua and A. Ushida, *A switching-parameter algorithm for finding multiple solutions of nonlinear resistive networks*, Int. J. Circuit Theory Appl. **4** (1976), no. 3, 215–237, DOI: https://doi.org/10.1002/cta.4490040302.
[49] L. O. Chua and N. N. Wang, *A new approach to overcome the overflow problem in computer-aided analysis of nonlinear resistive circuits*, Int. J. Circuit Theory Appl. **3** (1975), no. 3, 261–284, DOI: https://doi.org/10.1002/cta.4490030305.
[50] L. Trajkovic, R. C. Melville, and S.-C. Fang, *Finding DC operating points of transistor circuits using homotopy methods*, 1991 IEEE Int. Symp. Circuits Syst. Singapore **2** (1991), 758–761, DOI: https://doi.org/10.1109/ISCAS.1991.176473.
[51] M. Tolikas, L. Trajkovic, and M. D. Ilic, *Homotopy methods for solving decoupled power flow equations*, 1992 IEEE Int. Symp. Circuits Syst. San Diego, CA, USA **6** (1992), 2833–2839, DOI: https://doi.org/10.1109/ISCAS.1992.230609.
[52] R. C. Melville, L. Trajkovic, S. -C. Fang, and L. T. Watson, *Artificial parameter homotopy methods for the DC operating point problem*, IEEE Trans. Comput.-Aided Des. Integr. Circuits Syst. **12** (1993), no. 6, 861–877, DOI: https://doi.org/10.1109/43.229761.
[53] A. Dyes, E. Chan, H. Hofmann, W. Horia, and L. Trajkovic, *Simple implementations of homotopy algorithms for finding DC solutions of nonlinear circuits*, 1999 IEEE Int. Symp. Circuits Syst. Orlando, FL, USA **6** (1999), 290–293, DOI: https://doi.org/10.1109/ISCAS.1999.780152.
[54] L. Trajkovic, *Homotopy Methods for Computing DC Operating Points*, Wiley, 1999.
[55] L. Kronenberg, W. Mathis, and L. Trajkovic, *Limitations of criteria for testing transistor circuits for multiple DC operating points*, Proc. 43rd IEEE Midwest Symp. Circuits Syst. Lansing, MI, USA **1** (2000), 148–151, DOI: https://doi.org/10.1109/MWSCAS.2000.951607.
[56] L. Trajkovic, *Homotopy Algorithms for Finding DC and Steady-State Solutions of Nonlinear Circuits*, Electronics and Signal Processing Summer Symposium-LEOS, British Columbia, Canada, 2002.
[57] L. Trajkovic, R. C. Melville, and S.-C. Fang, *Improving DC convergence in a circuit simulator using a homotopy method*, Proc. IEEE 1991 Custom Integr. Circuits Conf. San Diego, CA, USA, 1991, pp. 8.1/1–8.1/4, DOI: https://doi.org/10.1109/CICC.1991.164032.
[58] L. Trajkovic, E. Fung, and S. Sanders, *HomSPICE: simulator with homotopy algorithms for finding DC and steady-state solutions of nonlinear circuits*, 1998 IEEE Int. Symp. Circuits Syst. Monterey, CA, USA **6** (1998), 227–231, DOI: https://doi.org/10.1109/ISCAS.1998.705253.
[59] H. Vazquez-Leal, A. Marin-Hernandez, Y. Khan, A. Yıldırım, U. Filobello-Nino, R. Castaneda-Sheissa, et al., *Exploring collision-free path planning by using homotopy continuation methods*, Appl. Math. Comput. **219** (2013), no. 14, 7514–7532, DOI: https://doi.org/10.1016/j.amc.2013.01.038.
[60] G. Diaz-Arango, H. Vazquez-Leal, L. Hernandez-Martinez, M. T. Sanz-Pascual, and M. Sandoval-Hernandez, *Homotopy path planning for terrestrial robots using spherical algorithm*, IEEE Trans. Autom. Sci. Eng. **15** (2017), no. 2, 567–585, DOI: https://doi.org/10.1109/TASE.2016.2638208.
[61] G. C. Velez-Lopez, H. Vazquez-Leal, L. Hernandez-Martinez, A. Sarmiento-Reyes, G. Diaz-Arango, and J. Huerta-Chua, et al., *A novel collision-free homotopy path planning for planar robotic arms*, Sensors **22** (2022), no. 11:4022, 1–27, DOI: https://doi.org/10.3390/s22114022.
[62] G. C. Velez-Lopez, L. Hernandez-Martinez, H. Vazquez-Leal, M. A. Sandoval-Hernández, V. M. Jimenez-Fernandez, and M. Gonzalez-Lee, *Collision-free path planning applied to multi-degree-of-freedom robotic arms using homotopy methods*, IEEE Access **12** (2024), 150702–150718, DOI: https://doi.org/10.1109/ACCESS.2024.3479095.
[63] M. L. Quemada-Villagómez, M. D. L. L. López-González, J. M. Oliveros-Muñoz, and H. Jiménez-Islas, *Ensennnanza del método de continuación homotópica con seguimiento hiperesférico para estudiantes de ingeniería*, Acta Univ. **32** (2022), 1–43, DOI: https://doi.org/10.15174/au.2022.3358.
[64] M. A. Sandoval-Hernández, H Vázquez-Leal, J. Huerta-Chua, U. A. Filobello-Nino, and D. Mayorga-Cruz, *La didáctica del cálculo integral: el caso de los procedimientos de integración*, Rev. Iberoam. Investig. Desarro. Educ. **13** (2022), no. 25, 1–28, DOI: https://doi.org/10.23913/ride.v13i25.1245.
[65] R. C. Uriza, G. M. Espinosa, and D. R. Gasperini, *Análisis del discurso matemático escolar en los libros de texto: una mirada desde la teoría socioepistemológica*, Av. Investig. Educ. Mat. **8** (2015), 9–28, DOI: https://doi.org/10.35763/aiem.v1i8.123.
[66] C. Prieto-De-Castro, *Biografía Henri Poincaré*, Instituto de Matemáticas, Universidad Nacional Autónoma de México, 1977.
[67] W. S. Massey, *Introdución a la Topología Algebraica*, Reverté, España, 2006.
[68] M. Macho-Stadler, *Homotopía, Publicaciones de divulgación*, Universidad del País Vasco-Euskal Herriko Unibertsitatea, 2003.
[69] J. Strom, *Modern Classical Homotopy Theory, Graduate Studies in Mathematics*, Vol. 127, American Mathematical Society, 2011.
[70] S. Lipschutz, *Theory and Problems of General Topology*, Schaumas Outline Series, Mc Graw-Hill, 1965.
[71] M. Macho-Stadler, *Qué es la Topología?*, Publicaciones de divulgación, Universidad del País Vasco-Euskal, Herriko Unibertsitatea, Euskadi, 2018, https://divulgacioncientificadecientificos.blogspot.com/2018/08/que-es-la-topologia-marta-macho-stadler.html.
[72] L. E. J. Brouwer, *Beweis des Jordanschen Kurvensatzes*, Math. Ann. **69** (1910), 169–175, DOI: https://doi.org/10.1007/BF01456867.
[73] L. E. J. Brouwer, *Über Abbildung von Mannigfaltigkeiten*, Math. Ann. Springer **71** (1911), 97–115, DOI: https://doi.org/10.1007/BF01456931.
[74] C. B. García and W. I. Zangwill, *Pathways to Solution Fixed Point in Equilibria*, Prentice Hall, 1981.
[75] J. Leray and J. Schauder, *Topologie et équations fonctionnelles*, Ann. Sci. Éc. Norm. Supér. **51** (1934), 45–78. http://www.numdam.org/item/10.24033/asens.836.pdf.
[76] F. A. Ficken, *The continuation method for functional equations*, Comm. Pure Appl. Math. **4** (1951), no. 4, 435–456, DOI: https://doi.org/10.1002/cpa.3160040405.

[77] C. B. Haselgrove, *The solution of non-linear equations and of differential equations with two-point boundary conditions*, Computer J. Oxford University Press **4** (1961), no. 3, 255–259, DOI: https://doi.org/10.1093/comjnl/4.3.255.
[78] D. F. Davidenko, *On the approximate solution of a system of nonlinear equations*, Ukr. Mat. Zh. **5** (1953), no. 2, 196–206.
[79] E. Lahaye, *Use Methode de Resolution daune Categorie deeeeeéquations Transcendentes*, C.R. Acad. Sci. Paris **198** (1934), 1840–1842.
[80] D. F. Davidenko, *On the new method of numerically integrating a system of nonlinear equations*, Dokl. Akad. Nauk SSSR **88** (1953), 601–604.
[81] W. C., Rheinboldt, *An adaptive continuation process for solving systems of nonlinear equations*, Univ. Md. Banach Cent. Publ. **3** (1978), no. 1, 129–142. http://eudml.org/doc/208686.
[82] P. Deuflhard, A Step Size *Control for Continuation Methods and its Special Application to Multiple Shooting Techniques*, Univertitat Hidelberg, Instiut für Angewandte Mathematik, Numerische Mathematik, Springer-Verlag, 1979.
[83] J. N. Lyness and B. J. J. McHugh, *Integration over multidimensional hypercubes I. A progressive procedure*, Comput. J. **6** (1963), no. 3, 264–270, DOI: https://doi.org/10.1093/comjnl/6.3.264.
[84] E. L. Allgower and K. Georg, *Introduction to numerical continuation methods*, Classics in Applied Mathematics, Springer-Verlag, Philadelphia, 2003.
[85] H. Jiménez-Islas, *Paquete Computacional Para la Solución de Sistemas de Ecuaciones no Lineales*, PhD thesis, Instituto Tecnológico de Celaya, 1988, DOI: https://doi.org/10.13140/RG.2.2.12052.31363, https://acortar.link/cPGvWn.
[86] A. Ushida and L. O. Chua, *Tracing solution curves of non-linear equations with sharp turning points*, Int. J. Circuit Theory Appl. **12** (1984), no. 1, 1–21, DOI: https://doi.org/10.1002/cta.4490120102.
[87] Y. Shinohara, *A geometric method of numerical solution of nonlinear equation and error estimation by Urabeas proposition*, RIMS Kyoto Univ. **5** (1969), no. 1, 1–9, DOI: https://doi.org/10.2977/PRIMS/1195194748.
[88] R. K. Brayton, F. G. Gustavson, and G. D. Hachtel, *A new efficient algorithm for solving differential-algebraic systems using implicit backward differentiation formulas*, Proc. IEEE **60** (1972), no. 1, 98–108, DOI: https://doi.org/10.1109/PROC.1972.8562.
[89] C. W. Gear, *The automatic integration of ordinary differential equations*, Commun. ACM **14** (1971), no. 3, 176–179, DOI: https://doi.org/10.1145/362566.362571.
[90] K. Yamamura, *Simple algorithms for tracing solution curves*, IEEE Trans. Circuits Syst. I Fundam. Theory Appl. **40** (1993), no. 8, 537–541, DOI: https://doi.org/10.1109/81.242328.
[91] R. W. Klopfenstein, *Zeros of nonlinear functions*, RCA Lab. N.J. ACM Digit. Libr. **8** (1961), no. 3, 366–373, DOI: https://doi.org/10.1145/321075.321080.
[92] E. Allgower and K. Georg, *Introduction to Numerical Continuation Methods*, Classics in Applied Mathematics, Springer-Verlag, Philadelphia, USA, 1990.
[93] J. C. Alexander and J. A. Yorke, *The homotopy continuation method: numerically implementable topological procedures*, Trans. Amer. Math. Soc. **242** (1978), 271–284, DOI: https://doi.org/10.1090/S0002-9947-1978-0478138-5.
[94] S. N. Chow, J. Mallet-Paret, and J. A. Yorke, *Finding zeros of maps: homotopy methods that are constructive with probability one*, Math. Comput. **32** (1978), 887–899, DOI: https://doi.org/10.1090/S0025-5718-1978-0492046-9.
[95] L. T. Watson, *Engineering applications of the Chow-Yorke algorithm*, Appl. Math. Comput. **9** (1981), no. 2, 111–133, DOI: https://doi.org/10.1016/0096-3003(81)90010-2.
[96] S. N. Chow, J. Mallet-Paret, and J. A. Yorke, *A homotopy method for locating all zeros of a system of polynomials*, Lecture Notes Math. **730** (1979). 77–88, DOI: https://doi.org/10.1007/BFb0064312.
[97] T. Y. Li, T. Sauer, and J. A. Yorke, *The Cheateras homotopy: an efficient procedure for solving systems of polynomial equations*, SIAM J. Numer. Anal. **26** (1989), no. 5, 1241–1251, DOI: https://doi.org/10.1137/0726069.
[98] J. D. Seader, M. Kuno, W. Lin, S. A. Johnson, K. Unsworth, and J. W. Wiskin, *Mapped continuation methods for computing all solutions to general systems of nonlinear equations*, Comput. Chem. Eng. **14** (1990), no. 1, 71–85, DOI: https://doi.org/10.1016/0098-1354(90)87006-B.
[99] M. Kuno and J. D. Seader, *Computing all real solutions systems of nonlinear equations with a global fixed-point homotopy*, Ind. Eng. Chem. Res. **27** (1988), no. 7, 1320–1329, DOI: https://doi.org/10.1021/ie00079a037.
[100] S. H. Choi and N. L. Book, *Unreachable roots for global homotopy continuation methods*, AIChE J. **37** (1991), no. 7, 1093–1095, DOI: https://doi.org/10.1002/aic.690370713.
[101] S. Khaleghi-Rahimian, F. Jalali, J. D. Seader, and R. E. White, *A new homotopy for seeking all real roots of a nonlinear equation*, Comput. Chem. Eng. **35** (2011), no. 3 403–411, DOI: https://doi.org/10.1016/j.compchemeng.2010.04.007.
[102] K. Yamamura, *A fixed-point homotopy method for solving modified nodal equations*, IEEE Trans. Circuits Syst. I Fundam. Theory Appl. **46** (1999), no. 6, 654–665, DOI: https://doi.org/10.1109/81.768822.
[103] D. M. Wolf and S. R. Sanders, *Multiparameter, homotopy methods for finding DC operating points of nonlinear circuits, IEEE Trans*. Circuits Syst. I Fundam. Theory Appl. **43** (1996), no. 10, 824–838, DOI: https://doi.org/10.1109/81.538989.
[104] M. Sosonkina, L. T. Watson, and D. E. Stewart, *Note on the end game in homotopy zero curve tracking*, ACM Trans. Math. Software **22** (1996), no. 3, 281–287, DOI: https://doi.org/10.1145/232826.232843.
[105] H. Vazquez-Leal, A. Marin-Hernandez, Y. Khan, A Yıldırım, U. Filobello-Nino, and R. Castaneda-Sheissa, et al., *Exploring collision-free path planning by using homotopy continuation methods*, Appl. Math. Comput. Elsevier **219** (2013), no. 14, 7514–7532, DOI: https://doi.org/10.1016/j.amc.2013.01.038.
[106] R. Burden and J. Faires, *Numerical Analysis*, 9th edn., Cengage Learning, Boston, 2011.
[107] S. C. Chapra and R. P. Canale. *Métodos Numéricos Para Ingenieros*, McGraw-Hill, Mexico, 2011.

[108] A. S. Sedra, K. C. Smith, T .C. Carusone, and V. Gaudet, *Microelectronic Circuits*, 8th edn., Oxford University Press, Oxford, 2020.
[109] R. Boylestad and L. Nashelsky, *Electrónica: teoría de circuitos y dispositivos electrónicos*, Pearson Educación, Mexico, 2009.
[110] R. L. Tokheim, *Digital Electronics*, Glencoe, Glencoe, UK, 1994.
[111] J. M. Angulo-Usategui, B. Garcia-Zapirain, I. Angulo-Martínez, and J. V. Sáez, *Microcontroladores avanzados dsPIC: controladores digitales de señales: arquitectura, programación y aplicaciones*, Thomson, Mexico, 2006.
[112] B. B. Brey, *Los microprocesadores intel: arquitectura, programación e interfaces*, Pearson-Prentice-Hall, Mexico, 2007.
[113] J. S. Thomsen and S. Schlesinger, *Analysis of nonlinear circuits using impedance concepts*, IRE Trans. Circuit Theory **2** (1955), no. 3, 271–278, DOI: https://doi.org/10.1109/TCT.1955.1085250.
[114] J. S. Thomsen, *Graphical analysis of nonlinear circuits using impedance concepts*, J. Appl. Phys. AIP Publishing **24** (1953), no. 11, 1379–1382, DOI: https://doi.org/10.1063/1.1721182.
[115] M. A. Sandoval-Hernández, H. Vazquez-Leal, U. A. Filobello-Nino, G. J. Morales-AlarcóN, G. C. Velez-LóPez, and R. CastañEda-Sheissa, et al., *Using Horner's algorithm to reduce computing times*, Int. J. Eng. Res. Technol. **12** (2023), no. 06, 325–331. https://www.ijert.org/research/using-horners-algorithm-to-reduce-computing-times-IJERTV12IS060143.pdf.
[116] H. Vazquez-Leal, M. A. Sandoval-Hernandez, J. L. Garcia-Gervacio, A. L. Herrera-May, and U. A. Filobello-Nino, *PSEM aproximations for both branches of Lambert W with applications*, Discrete Dyn. Nat. Soc. **2019** (2019), 267951, DOI: https://doi.org/10.1155/2019/8267951.
[117] L. T. Watson, *A globally convergent algorithm for computing fixed-points of C^2 maps*, Appl. Math. Comput. **5** (1979), no. 4, 297–311, DOI: https://doi.org/10.1016/0096-3003(79)90020-1.
[118] H. Mohamad-Nor, A. Rahman, A. I. Md-Ismail, and A. Abdul-Majid, *Super Ostrowski homotopy continuation method for solving polynomial system of equations*, Matematika **32** (2016), no. 1, 53–67, DOI: https://doi.org/10.11113/matematika.v32.n1.685.
[119] H. Mohamad-Nor, A. I. Md-Ismail, and A. Abdul-Majid, *Linear fixed-point function for solving system of polynomial equations*, AIP Conf. Proc. **1602** (2014), no. 1, 105–112, DOI: https://doi.org/10.1063/1.4882474.
[120] S. Sutherland, *An introduction to Julia and Fatou sets*, in: Fractals, Wavelets, and their Applications: Contributions from the International Conference and Workshop on Fractals and Wavelets, vol. 92, Springer Proceedings in Mathematics & Statistics, Switzerland, 2014, pp. 37–60.
[121] G. N. Rubiano, *Método de Newton, Mathematica y fractales: historia de una página*, Bol. Mat. **14** (2007), no. 1, 44–63.
[122] K. Madhu and J. Jayaraman, *Higher order methods for nonlinear equations and their basins of attraction*, Mathematics **4** (2016), no. 2, 22, DOI: https://doi.org/10.3390/math4020022.
[123] B. Haible and R. B. Kreckel, *CLN, A Class Library for Numbers*, GiNaC C++ library, Germany, 1996. https://www.ginac.de/CLN/cln.pdf.
[124] P. R. Bell and J. M. Doughertym, *Nonlinear image processing method*, IEEE Trans. Nucl. Sci. **25** (1978), no. 2, 928–938, DOI: https://doi.org/10.1109/TNS.1978.4329438.
[125] H. Daisuke, E. Takaya, M. Kadowaki, Y. Kobayashi, and T. Ueda, *Effect of the pixel interpolation method for downsampling medical images on deep learning accuracy*, J. Comput. Commun. **9** (2021), no. 11, 150–156, DOI: https://doi.org/10.4236/jcc.2021.911010.
[126] A. Singh and J. Singh, *Review and comparative analysis of various image interpolation techniques*, 2019 IEEE 2nd Int. Conf. Intell. Comput. Instrument. Control Technol. Kannur, India **1** (2019), 1214–1218, DOI: https://doi.org/10.1109/ICICICT46008.2019.8993258.